Catastrophic Hydraulic Failure and Tipping Points in Plants

Daniel M. Johnson[1], Gabriel Katul[2,3], and Jean-Christophe Domec[3,4]

[1]*Warnell School of Forestry and Natural Resources, University of Georgia, Athens GA 30602 USA*

[2] *Department of Civil and Environmental Engineering, Duke University, Durham NC 27708 USA*

[3]*Nicholas School of the Environment, Duke University, Durham, North Carolina 27708 USA*

[4]*Bordeaux Sciences Agro, UMR INRA-ISPA 1391, 33195, Gradignan, France*

Author for correspondence:
Daniel M. Johnson
Warnell School of Forestry and Natural Resources
University of Georgia
Athens GA 30602
danjohnson@uga.edu

Abstract:

Water inside plants forms a continuous chain from water in soils to the water evaporating from leaf surfaces. Failures in this chain result in reduced transpiration and photosynthesis and these failures are caused by soil drying and/or cavitation-induced xylem embolism. Xylem embolism and plant hydraulic failure share a number of analogies to "catastrophe theory" in dynamical systems. These catastrophes are often represented in the physiological and ecological literature as tipping points or alternative stable states when control variables exogenous (e.g. soil water potential) or endogenous (e.g. leaf water potential) to the plant are allowed to slowly vary. Here, plant hydraulics viewed from the perspective of catastrophes at multiple spatial scales is considered with attention to bubble expansion (i.e. cavitation), organ-scale vulnerability to embolism, and whole-plant biomass as a proxy for transpiration and hydraulic function. The hydraulic safety-efficiency tradeoff, hydraulic segmentation and maximum plant transpiration are examined using this framework. Underlying mechanisms for hydraulic failure at very fine scales such as pit membranes, intermediate scales such as xylem network properties and at larger scales such as soil-tree hydraulic pathways are discussed. Lacunarity areas in plant hydraulics are also flagged where progress is urgently needed.

Keywords: bifurcation, cavitation, cusp, embolism, fold, r-shaped curves, s-shaped curves, soil, transpiration, water potential, xylem

Introduction:

To cool leaves and enable photosynthesis in a desiccating atmosphere, plants must loose large amounts of water through stomatal openings distributed on leaf surfaces. The water vapor loss from leaves is replenished by liquid water that travels through the plant from soil pores. The voluminous water loss becomes apparent when recognizing that more than 95% of the water taken up by roots exits the plant in the form of water vapor through stomatal pores that cover less than 2% of the total leaf area (Bertolino et al., 2019). The delivery of water from soil to leaves needed to sustain photosynthetic demand occurs through a system of water-conducting channels called xylem. Water molecules within the xylem are held together by electromagnetic (van der Waal) forces resulting from positive and negative charges of hydrogen and oxygen atoms (hydrogen bonds) making up water molecules. These forces endow water with two properties: (i) weak compressibility because the van der Waal forces become repulsive at very small separation distances between water molecules and (ii) cohesiveness as the van der Waal forces become attractive after a certain threshold distance separating water molecules is crossed. The cohesiveness allows water to remain liquid even under tension. It has eluded Francis Darwin who argued that "*To believe that columns of water should hang in the tracheals like solid bodies, and should, like them, transmit downwards the pull exerted on them at their upper ends by the transpiring leaves, is to some of us equivalent to believing in ropes of sand*" (Darwin, 1896). Today, the accepted theory, known as cohesion tension theory (Dixon & Joly, 1894), envisions a water column within the xylem resembling a 'chain' of interconnected water molecules. This

chain is anchored to the parenchyma tissue of a leaf on one end and to the root-water on the other (van den Honert, 1948; Konrad et al., 2019). For every water molecule lost to the atmosphere from leaves, the entire chain must be pulled up a distance of one water molecule (Konrad et al., 2019) thereby increasing the tension on the chain. Undoubtedly, the ability of plants to passively move water upwards over long distances against the gravitational pull and frictional forces resulting from adhesion of water molecules onto the xylem walls without active pumping remains supreme in energy-efficient water delivery. However, in periods of less than abundant root-zone soil water, this energy efficiency in water transport comes at a price – rapid water tension buildup. Water under tension is in a metastable state, meaning that its hydrostatic pressure is below the saturation vapor pressure. In such a metastable state, any disturbance (mechanical or otherwise) can lead to the formation of vapor-filled bubbles, a phenomenon known as cavitation. In the absence of such external disturbance (e.g. mechanical agitation), pure water (i.e. free of contaminants or air bubbles) in a metastable state can be 'stretched' up to 150 MPa at room temperature ($\sim$ 300 K) before vapor-filled bubbles spontaneously form (Oertli 1971; Konrad et al., 2019). This high tension is a testament to the maximum attractive strength of the van der Waal forces. Xylem tension in plants is well below 150 MPa, which is why bubble formation in plants is not attributed to this mechanism (also known as homogeneous nucleation; Briggs, 1950; Konrad et al., 2019).

Xylem conduits are the remnants of living cells that lost their protoplast and thus are water-filled and above all, air bubble-free. However, the unavoidable presence of some leaks and cracks, which can be induced by simply breaking off a twig or a leaf, or by insect feeding exposing sapwood, within the xylem cell walls allows a group of air molecules to enter some water filled conduits. These air molecules enable tiny embryonic bubbles to form and potentially grow within the infected conduit (vessel or tracheid) at tensions 1-2 orders of magnitude smaller than 150 MPa (Konrad et al., 2019). When the expanding forces exceed the restoring forces at the bubble interface, the embryonic bubble expands to fill most (but not all) of the conduit (Konrad and Roth-Nebelsick, 2006). The *spread of embolism* within the xylem results from air seeding at inter-conduit pit membranes rather than new cavitation events in the bulk phase of the sap (Fig. 1; Zimmermann, 1983). Air seeding actually occurs from those expanded bubbles being pulled through pore openings or through ruptures in pit membranes (Fig. 1 a,b; vessel air-seeding; Sperry & Hacke, 2004), or when the pit membrane is stretched beyond the point of rupture (tracheid air-seeding; Domec et al., 2006; Delzon et al. 2010). Fortunately, xylem cell redundancy maintains adequate water transport, even following multiple air seeding events (Mrad et al., 2021). More problematic for the xylem is that air has low solubility in water. Air molecules (primarily nitrogen) trapped within embryonic bubbles cannot rapidly dissolve by condensation when tension in the xylem drops. To the contrary, water vapor molecules trapped within the bubble can condense almost instantly. Thus, depending on the number of air molecules within an embryonic bubble, these molecules can act to destabilize the bubble with further increases in xylem tension leading to embolism spread (i.e. blocking of xylem vessels or tracheids by air bubbles; Figure 2) and subsequent hydraulic failure (i.e. loss of overall conductivity of the water delivery network). Embryonic air bubbles of size < 1 nanometer (1×10^{-9}m) can initially grow with increased tension enough but remain stable and initially harmless. Beyond a certain bubble size and when in abundance, these air bubbles can push water

molecules apart by sufficient distances to weaken the van der Waal attractive forces needed for maintaining cohesion. The mean distance between water molecules is 0.3×10^{-9}m and for simplicity is assumed to be comparable to the 'equilibrium distance' where the overall electric potential is minimum. At distances between water molecules far exceeding 0.3 nanometers, the van der Waal attractive forces decay as an inverse 6-th power (instead of inverse square) though it is worth noting that the repulseive forces increase as inverse 12-th power for separation distances smaller than 0.3 nanometer. Weakening of the attractive forces by the presence of air bubbles can result in loss of cohesion among water molecules. In this situation, the chain defining the water column becomes even more prone to breaking under tension ultimately leading to overall hydraulic failure.

Hydraulic failure is commonly associated with plant mortality and there are many examples (Sevanto et al., 2014; Adams et al., 2017; Rowland et al., 2015; Hammond et al., 2019). Drought induced tree mortality has been observed across the globe (Allen et al., 2010; Allen et al., 2015). Projected changes in mean air temperatures and precipitation alter the balance between supply and demand for water needed to sustain photosynthesis (Manzoni et al., 2014). Searching for tipping points that lead to frequent hydraulic failures and ultimately drought-induced mortality from shift in statistics derived using long-term satellite records of leaf area proved to be successful (e.g. Liu et al., 2019, 2020). Yet, the genesis of the collapse of the plant water transport is amenable to a deterministic treatment, which frames the scope of this review.

Here, a multi-scale framework based on catastrophe theory to measure ecological risk of embolism is proposed. The assessment models involve multiple spatial scales that cover the status of bubble formation and expansion, embolism spread in xylem and soil, and the hydraulic effects of embolism for plant functioning under changing climate (Fig. 1). The results provide guidance for the risk assessment of environment for the strong objectivity of catastrophe theory compared with other evaluation methods. The time is ripe for this undertaking given (i) the proliferation of remote sensing products (NDVI for plants, SMAPS for near-surface soil moisture and plant water storage, ECOSTRESS for estimating canopy transpiration), (ii) the availability of accessible past, present, and projections of large-scale hydroclimatic variables (e.g. air temperature, water vapor, and precipitation through NCEP re-analysis), and (iii) wealth of experiments and global public data bases on plant water use (SAPFLUXNET) and hydraulics traits across biomes and species (TRY database, XFT database).

What is Catastrophe Theory?

Hydraulic failure at multiple scales leading to plant mortality shares some resemblance to "catastrophe theory" in dynamical systems (Thom, 1975; Zeeman, 1976; Parolari et al., 2014; Manzoni et al., 2014; Konrad & Roth-Nebelsick, 2003; Konrad et al., 2019; see also Zeeman, 1978 video). In catastrophe theory, a single differential equation or a set of differential equations represent the temporal evolution of the state variable of the system (e.g. biomass, soil or plant water status, bubble size, etc.). The parameters of these equations needed to describe the temporal trajectory of the state variables are labelled "control parameters". In plant hydraulics, these control variables may be exogenous, such as air molecules that enter a xylem conduit or vapor pressure deficit in the atmosphere, or endogenous, such as xylem tension. Equilibrium points, also known as stagnation points or steady-state limits, can be derived as a function of

these control variables. Gradual variations in these control variables due to a prolonged drought, slow changes in soil nutritional status, gradual increase in elevated atmospheric CO_2, or age-related factors can lead to sudden shifts in the stability of an existing equilibrium point or appearance and disappearance of equilibrium points. The slow variations in these control parameters are 'endogenous' to the dynamical system and differ from 'exogenous' disturbances (or shocks) acting on the ecosystem (i.e. ice storm or hurricane diminishing leaf area or plant biomass, forest fires, etc.). When ignoring these exogeneous disturbances and assuming that the control parameters can be treated as pre-determined constants to be dialed up or down depending on external conditions, the resulting dynamical system is labeled as 'autonomous' and time is no longer an explicit variable.

Conceptually, ecosystems exist in equilibrium states ranging from deserts (i.e. small plant biomass per unit ground area) to tropical forests (plant biomass per unit ground area is large) depending on long-term rainfall amounts and air temperature (control variables). Catastrophe theory is effective in identifying or delineating "tipping points" in the control variables that alter the equilibrium properties of the dynamical system derived for these control parameters as the control parameters are dialed up or down. The study of fluid dynamics is full of such examples such as the transition from laminar to turbulent flow where the Reynolds number is the control variable, transition from supercritical to subcritical state through a hydraulic jump where the Froude number is the control variable, or the emergence of convection cells where the Rayleigh number is the control variable. In ecosystems, a dramatic case is when a desertification state switches from being an unstable equilibrium point to being a stable equilibrium (Konings et al., 2010). The occurrence of multiple equilibrium points (or alternative stable states) and loss or alteration of their stability is linked to the nature of the non-linearity governing the system (Strogatz, 1994). It is a topic with long-standing tradition in the ecological sciences (Scheffer et al., 2001, 2003). The linkage between equilibrium points (and their stability) and the variations in control parameters as they are increased or decreased is formally studied using 'bifurcation analysis' and is the corner stone of catastrophe theory. This analysis is illustrated in Box 1 by considering an isolated plant whose above ground biomass (B) dynamics is represented by the von Bertalanffy equation (VBE). Many of the phenomena in the plant world, from patterns of tree mortality (Dietze & Moorcroft, 2011) to xylem loss of hydraulic conductivity (Sperry et al., 1994) and spruce budworm outbreak (Ludwig et al., 1978) are non-linear in nature and often display similarities to the catastrophe.

BOX 1: Carbon Balance, Bifurcation Analysis, and the von Bertalanffy Equation (VBE)

The VBE is given by (von Bertalanffy, 1938; Perry, 1984; Mrad et al., 2020; see Table 1 for symbol definitions)

$$\frac{dB}{dt} = A_c\, P_g\, L - k_m B,$$

where B is above-ground biomass, t is time, A_c is the proportion of photosynthates allocated to above ground tissue, P_g is the gross photosynthesis per unit leaf area reduced by photorespiration and synthesis respiration, L is the leaf area of the individual plant, and k_m is rate of maintenance respiration plus tissue death. The VBE assumes that a plant harvests

resources (photosynthetically active radiation here) through a surface area proportional to L but incurs respirational costs proportional to its biomass (or volume). When naively setting $L = c\ B^n$ dictated by allometric relations defined by parameter c and scaling exponent n, the VBE can be expressed as a single-equation dynamical system given by

$$\dot{B} = \frac{dB}{dt} = f(B) = (A_c\ P_g\ c)\ B^n\ -\ k_m B = k_m B\ \left(\frac{A_c\ P_g\ c}{k_m} B^{n-1}\ -\ 1\right)$$
$$= k_m B\ (\alpha\ B^{n-1}\ -\ 1)\ ,$$

where the overdot indicates differentiation with respect to time as common in the dynamical systems literature (Strogatz, 1994), $\alpha = A_c\ P_g\ c/k_m,\ n,$ and k_m are plant-specific positive constants and $\dot{B} = f(B)$ is the dynamical system describing the time trajectories of above-ground biomass given by the VBE. Von Bertalanffy labelled the constant terms $(A_c\ P_g\ c)$ and k_m as coefficients of anabolism and catabolism, respectively. Returning to the specific trajectory (also known as the particular solution) of the dynamical system $\dot{B} = f(B)$ in time, it requires the specification of $\alpha,\ n,$ and k_m as well as an initial condition - the biomass at t=0 or $B(0)$. The study of dynamical systems enables the exploration of many properties of the VBE without actually solving this differential equation. By focusing on key points such as the equilibrium or steady-state points, it is possible to assess the long-term responses of the dynamical systems in relation to the control variables of $\alpha,\ n$ and $k_m$without detailed knowledge of the time trajectory from the initial state to the steady-state. The response of a plant to an extended drought occurs at multiple time scales (Hsiao, 1973). On physiological time scales (i.e. time scales commensurate with stomatal opening and closure), droughts reduce the hydraulic capacity of the xylem to deliver water so as to sustain the biochemical demand for carbon dioxide thereby reducing the value of P_g. On intermediate time scales (i.e. allocation of carbon), A_c is reduced so as to allocate more carbon to belowground tissue construction needed for enhancing access to water and nutrients in the soil. On even longer time scales, foliage shedding occurs reducing L and altering the allometry linking L to B by adjusting c and/or n. Likewise, α and n can vary with elevated atmospheric CO_2 or nutritional status of the soil. When these parameters vary slowly in time (e.g. due to climate change), then they can be treated as control variables in the VBE thereby making this dynamical system autonomous.

Equilibrium (or steady-state) in the VBE is attained upon setting $\dot{B} = 0$ and the relation between the control variables α and n and the emergence and stability changes of these equilibrium points is the backbone of catastrophe theory. There are only two equilibrium states for the VBE: $B_{eq,1} = 0$ (i.e. death or extinction) and $B_{eq,2} = \alpha^{1/(n-1)}$ (finite biomass). These two equilibrium points may be either stable or unstable depending on the numerical value of α and n. The case where L scales linearly with aboveground biomass ($n = 1$) leads to loss of all non-linearities and only one equilibrium point exists: $B_{eq,1} = 0$. For $\alpha > 1$, this equilibrium point is unstable and B grows exponentially as $t \to \infty$. For $\alpha < 1$, this equilibrium point is stable and is asymptotically approached as $t \to \infty$.

The dynamically interesting case is when $n \neq 1$ where the stability of the two equilibrium points $B_{eq,1} = 0$ and $B_{eq,2} = \alpha^{1/(n-1)}$ can be assessed using linear analysis. In linear analysis, a small biomass perturbation δB to the equilibrium state (B_{eq}) is introduced and its growth or decay in time is then analyzed. Setting $B = B_{eq} + \delta B$ and recalling that $\dot{B} = f(B)$, the dynamical system can be expressed as

$$\dot{B_{eq}} + \dot{\delta B} = f(B_{eq} + \delta B) = f(B_{eq}) + \frac{d}{dB} f(B)\Big|_{B_{eq}} \delta B + H.O.T,$$

where H.O.T. stands for higher-order terms of the Taylor series expansion applied to $f(B_{eq} + \delta B)$ around B_{eq}. At equilibrium, $\dot{B_{eq}} = f(B_{eq}) = 0$ resulting in

$$\dot{\delta B} = \frac{d}{dB} f(B)\Big|_{B_{eq}} \delta B = f'(B_{eq})\, \delta B,$$

where primed quantities indicate differentiation with respect to the state variable B (instead of time). Hence, the evolution of the biomass perturbation around the B_{eq} is governed by

$$\frac{\dot{\delta B}}{\delta B} = f'(B_{eq}).$$

Provided $f'(B_{eq}) \neq 0$, δB grows exponentially in time away from $B_{eq}$when $f'(B_{eq}) > 0$ (i.e. B_{eq} is an unstable equilibrium) and decays exponentially in time back to B_{eq} when $f'(B_{eq}) < 0$ (i.e. B_{eq} is a stable equilibrium).

For the VBE,

$$f'(B_{eq}) = k_m(n\, \alpha\, {B_{eq}}^{n-1} - 1).$$

In the case of $B_{eq,2} = \alpha^{1/(n-1)}$,

$$f'(B_{eq,2}) = k_m(n - 1).$$

Interestingly, the stability of $B_{eq,2}$ only depends on the degree of non-linearity *n* set by the allometric relation between *B* and *L*. For $n > 1$, $B_{eq,2}$ is unstable whereas for $n < 1$, this equilibrium biomass is stable. For many species, the reported $n = 0.46 - 0.88$ (mean of $n = 0.84$) with the lower range of n associated with species that are highly intolerant to shade and conversely (Perry, 1984). This range is consistent with the stability requirement that $n < 1$ for a non-extinction equilibrium to exist (i.e. $B_{eq,2} = \alpha^{1/(n-1)}$). Interestingly, von Bertalanffy determined an $n = 2/3$ and was of the opinion that this value is universal for all vertebrates. For plants, a mean $n = 0.84$ exceeding 2/3 may be anticipated given that plant foliage harvest photosynthetically active radiation in three-dimensions instead of the near-two dimensions for vertebrates.

Returning to the stability of $B_{eq,1} \to 0^+$ (i.e. death or extinction) approached from a positive biomass end,

$$f'(B_{eq,1}) = k_m[n\, \alpha\, (0^+)^{n-1} - 1].$$

For $n < 1$, $B_{eq,1} = 0$ is unstable (i.e. $f'(B_{eq,1}) > 0$) whereas for $n > 1$, $B_{eq,1} = 0$ is stable (i.e. $f'(B_{eq,1}) < 0$). When $B > B_{eq,2}$ and $n > 1$, the dynamical system does not go back to $B_{eq,2}$ but exhibits a so-called 'finite-time' singularity - meaning that biomass blows up ($i.e. B \to \infty$) in a finite amount of time. In this case, the VBE reduces to the much-studied 'doomsday' equation (von Foerester, 1960; Sornette, 2002; Kaack and Katul, 2013; Parolari et al., 2015).

In catastrophe theory, the visualization of the stability of equilibrium points is aided when they are placed on a so-called 'potential surface' (Zeeman, 1976; Strogatz, 1994). This surface is specified by a function $V(B)$ and is mathematically given as

$$\dot{B} = f(B) = -\frac{dV}{dB} = -V'(B).$$

The term 'potential' originates from the fact that B represents a biomass position (on the real line), $\dot{B}$ is thus analogous to a change in position with respect to time or a velocity, and $f(B)$

may be viewed as analogous to an external force that is balanced by linear friction per unit mass (i.e. $\dot{B}$) when viewed from the force balance $\dot{B} = f(B)$. Taking this analogy one step further, $dV = -f(B)dB$ becomes analogous to incremental work defined by the product of the aforementioned external force $f(B)$ acting on the system and the incremental distance dB. The negative sign in $dV = -f(B)dB$ is needed to ensure that

$$\dot{V} = \frac{dV}{dt} = \frac{dV}{dB}\frac{dB}{dt} = -f(B)\frac{dB}{dt} = -\left(\dot{B}\right)^2.$$

Hence, $\dot{V}$ always decreases with increasing time until reaching $\dot{B} = 0$ (i.e. equilibrium point) via a trajectory that always follows a path of decreasing potential.

For the VBE,

$$V(B) = -\int f(B)dB = \frac{1}{2}k_m B^2\left(1 - \frac{2\alpha}{1+n}B^{n-1}\right) + C_1,$$

where C_1 is an integration constant that can be set to zero (or any arbitrary number). The potential surface for $n = 0.84$ (mean value across many species) and $n = 1.2$ while maintaining $\alpha = 0.95$ the same are shown in the Fig. B1. The $B_{eq,2}$ is a stable equilibrium for $n = 0.84$ (as expected) whereas extinction or death is unstable as evidenced by the curvature of $V(B)$. For $n = 1.2$ the curvatures shift and the $B_{eq,2}$ is no longer stable whereas extinction now is. This shift in stability of the two equilibrium points as n transitions from sub-unity to super-unity is a hallmark of what is known as 'transcritical bifurcation' where stability points do not appear or disappear. They only alter their stability with respect to the control variable (here n) as they cross $n = 1$. Thus, the VBE illustration makes the link between bifurcation type (transcritical) and the degree of non-linearity (n) characterizing the dynamical system explicit.

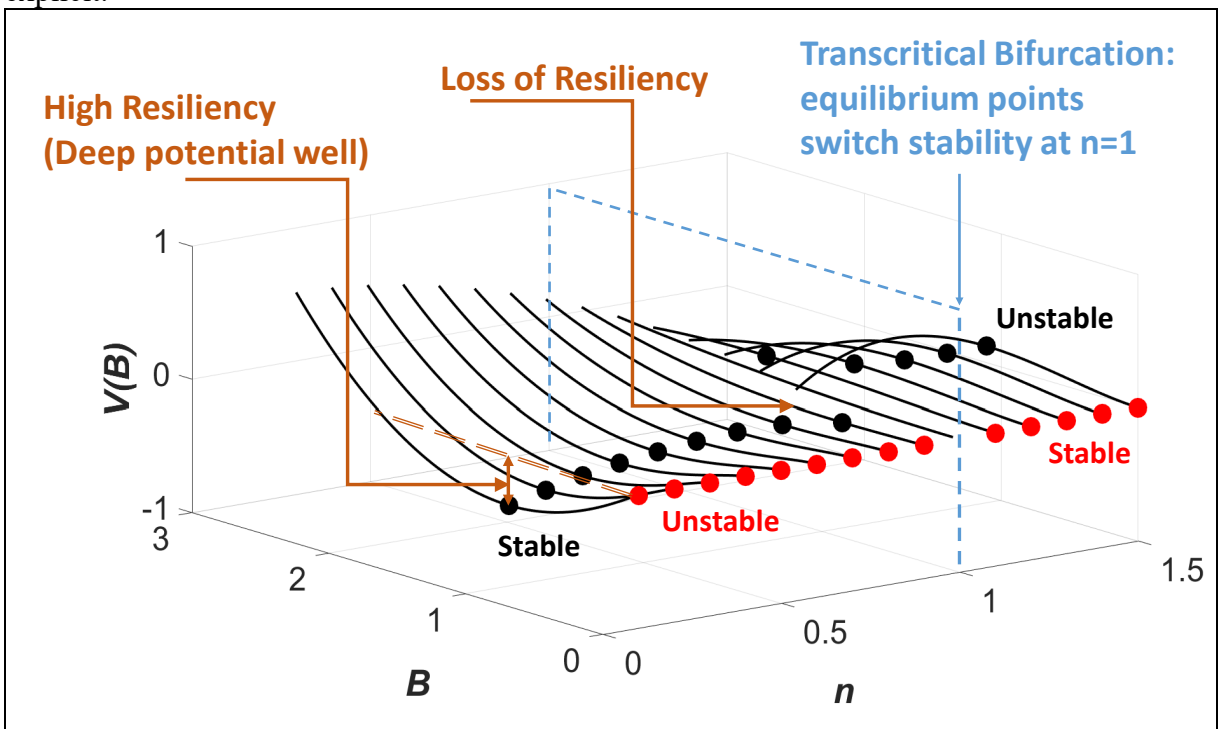

Figure B1: The variations of the potential surface $V(B)$ with B and n for $\alpha = 0.95$ The two equilibrium points $B_{eq,2} = \alpha^{1/(n-1)}$ and $B_{eq,1} = 0$ are shown as black and red circles, respectively. Based on the convexity of $V(B)$, the equilibrium state for $B_{eq,1}$ and $B_{eq,2}$ can

be determined. For $n < 1$, $B_{eq,2}$ is stable whereas $B_{eq,1} = 0$ is unstable. For $n > 1$, the stability of these equilibrium points reverses. Thus, a 'catastrophe' occurs when n transitions from sub-unity to super-unity. This bifurcation on the control parameter n is known as 'trans-critical' because no new equilibrium points are produced (or lost) – only their stability is exchanged with n crossing a critical value of unity. This catastrophe is termed as 'fold' (Zeeman, 1976). The resiliency of this system is high because there is only one stable equilibrium point (instead of multiple stable equilibria). However, as the critical n=1 is approached, the potential surface at $B_{eq,2}$ becomes shallower and shallower and at n=1, it becomes entirely flat resulting in a collision between the two equilibrium points followed by a shift in their stability. That the potential is becoming shallower as the critical n is approached is a signature of loss of resiliency – and can be used as an early warning signal of an impending catastrophe (in this case, a zero above ground biomass, i.e. plant death).

Hydraulic failure and Catastrophes: From bubble to whole-plant

The connection between catastrophe theory and hydraulic failure in plants has been receiving some attention in various forms and across scales spanning single bubble, whole plants and forests. The work here aims to show similarities in the catastrophe across scales, highlight the control variables, and expand upon the processes needed to describe the control variables and the mechanisms they espouse to represent. To illustrate catastrophe theory at all these scales, the approaches in Konrad & Roth-Nebelsick (2003) and Manzoni et al., (2014) are used.

Bubble Scale:

The connections between catastrophe theory and hydraulic failure at the bubble scale commences with an isolated spherical bubble of initial radius R that appears in a xylem conduit. The focus is not on how 'pioneering' air molecules entered a particular xylem conduit but whether the bubble radius will expand or contract depending on the expanding versus contracting forces acting on the bubble. If the 'pioneering' air molecules result in bubble radii that are unstable, the bubble may expand or even explode (and release acoustic energy; e.g., Millburn & Johnson, 1966). The infected conduit fills up rapidly with air (and water vapor) and becomes hydraulically dysfunctional. If the adjacent conduit is hydraulically functional, the air molecules can then spread from the dysfunctional to the functional conduit depending on the membrane properties and their state separating the two conduits. The ease of spread of air molecules from dysfunctional to functional conduits in this manner is the essence of the so-called air-seeding hypothesis (Zimmermann, 1983).

Returning to the pioneering air molecules infecting an isolated conduit, the control parameters here are the background xylem pressure and the molecular composition of the bubble. Thus, the stability of the bubble radius forms the basis of a dynamical system that is shown to exhibit a catastrophe when these control parameters are slowly varied. These control variables are background liquid xylem pressure p_s (i.e. negative or positive for now), initial R (bubble radius), and the amount of molecules or particle number n (including air, water vapor, and other

gases) trapped inside the bubble. The initial volume of the bubble $V = (4/3)\pi R^3$ and the initial surface area $A = 4\pi R^2$.

Throughout, it is assumed that the bubble and the liquid water in the xylem are in *thermal equilibrium* so that the temperature *T* is the same throughout and no heat exchange occurs. *Mechanical equilibrium* requires that the gas pressure inside the bubble (p) act in an outward directed force be balanced by the pressure at the bubble interface. Absence of a mechanical equilibrium leads to rapid changes in bubble radius and necessitates the inclusion of viscous forces, local and advective acceleration terms resulting in the Rayleigh-Plesset equation(see Plesset and Prosperetti, 1977; Holtta et al., 2007). However, at equilibrium, p is balanced by surface tension (=$2\gamma/R$ where γ =72 mN m^{-1} at standard temperature is the surface tension coefficient of liquid water expressed in force per unit length) that acts to contract the bubble and background xylem liquid pressure p_s that acts to expand (when in tension) or contract (when in compression) the bubble. Thus, the force balance leads to

$$p = p_s + \frac{2\gamma}{R},$$

which is the Young-Laplace equation. When $p > p_s + \frac{2\gamma}{R}$, the bubble grows whereas when $p < p_s + \frac{2\gamma}{R}$, the bubble contracts. At equilibrium, *p* is higher than p_s of the surrounding liquid. Note that in xylem conduits p_s is generally lower than *p*, and as p_s becomes more negative (increased tension) the bubble radius will decline thus potentially allowing the bubble to spread (air-seeding) if it drops below the radius of the pit membrane pores. To illustrate typical bubble sizes, consider a bubble pressure that is close to atmospheric (=+0.1 MPa) and $p_s = -2$ MPa (typical operating xylem pressure), equilibrium leads to bubble sizes that are on the order of

$$R = \frac{2\gamma}{p - p_s} = 0.06\ \mu m,$$

or some 230 times the mean distance between water molecules. In general, the pressure p inside the bubble depends on n and T when not atmospheric. To proceed further, it is assumed that the gas in the bubble is ideal so that (Konrad & Roth-Nebelsick; 2003)

$$n(R) = \frac{pV}{\Re\, T} = \frac{4\pi}{3\Re\, T} R^3 \left(p_s + \frac{2\gamma}{R}\right) = \frac{4\pi}{3\Re\, T}(p_s R^3 + 2\gamma R^2),$$

where $\Re = 8.314$ m^3 Pa mol^{-1} K^{-1} is the universal gas constant. This expression has an equilibrium point at R=0 (irrespective of p_s) where $n(R) = 0$ and the embryonic bubble is assumed to have dissolved in the xylem (i.e. safe). Stability of the bubble can now be assessed based on the initial number of particles n_i trapped in the bubble at some initial radius R when referenced to the maximum allowed $n(R)$.

When $p_s > 0$ (as may be expected at night when the soil is near saturation), $n(R)$ is a monotonically increasing function of R. Thus, when n_i differs from n(R), the bubble will simply expand (when $n_i > n(R)$) or contract (when $n_i < n(R)$) until the equilibrium point $n_i = n(R)$ is reached. However, this equilibrium point remains a stable equilibrium point and the radius of

the bubble simply adjusts until $n_i = n(R)$ at this equilibrium. There is no catastrophe associated with this positive xylem pressure state.

When $p_s < 0$ (typical of xylem pressures during the day when transpiration or water stress occurs), the situation is different. A new equilibrium is created as p_s changes from positive to negative. This new equilibrium point can be determined when $n(R)$=0 and requires $p_s R^3 + 2\gamma R^2 = 0;\ R_e = -2\gamma/p_s > 0$. This is the maximum possible radius that can be reached by the bubble under tension p_s without bubble bursting (Konrad & Roth-Nebelsick, 2003).

The maximum number of molecules n_{max} that can be accommodated at any $p_s < 0$ can also be computed by setting

$$\frac{dn}{dR} = \frac{4\pi}{3\Re\, T}(3p_s R^2 + 4\gamma R) = 0,$$

solving for the radius

$$R_m = \frac{-4\gamma}{3p_s},$$

and inserting this estimate of the radius into the $n(R)$ yields (Konrad & Roth-Nebelsick, 2003)

$$n_{max}(R_m) = \frac{2\pi\gamma}{\Re\, T}\left(\frac{8\gamma}{9p_s}\right)^2.$$

Three cases are considered:

These three regimes are similar to those derived from thermodynamic considerations discussed elsewhere (Shen et al., 2002, 2003, 2012; Konrad & Roth-Nebelsick, 2005).

The analysis thus far assumed that only air molecules occupy the bubble. When an embryonic bubble forms, liquid water molecules in contact with the bubble surface vaporize instantly into the bubble until the saturation vapor pressure (p^*) is reached inside the bubble. Because saturation vapor pressure is only dependent on T, and the analysis thus far assumes thermal equilibrium, p^* can be approximated from the Clausius-Clayperon equation. This pressure is, for all practical purposes, contributing to the expansion force of the bubble. Hence, the presence of water vapor molecules may be accommodated by replacing p_s with $p_s - p^*$. In the case when p_s is negative (tension), inclusion of water vapor molecules increase the apparent tension by an extra p^* that surface tension has to now resist. Roughly, for T = 20 C, the Clausius-Clayperon estimates $p^* \approx 2.5\ kPa$ but typical p_s in the xylem during droughts is on the order of -1 MPa. Hence, the role of water vapor molecules can be ignored at xylem tensions exceeding 0.1 MPa though it can be included for completeness in any stability analysis by replacing p_s with $p_s - p^*$. Last, bubbles that make contact with flat vessel walls (when $p_s < 0$) require energy to detach and experience weakening of the restoring force due to finite contact angles (i.e. γ becomes $\gamma\cos(\theta)$ where θ is the contact angle). In the case of non-flat wall vessels, other factors may become significant and can mitigate some this adverse effect (Konrad & Roth-Nebelsick, 2009).

There are a number of counteracting effects that play a role in mitigating the effect of unstable bubble growth. With rapid bubble expansion, an expanding bubble may isolate some water in the embolized vessel from the intact vessel. Due to its incompressibility, the trapped water in the embolized vessel begins to experience a reduction in tension or even a local positive pressure (in contrast to the negative pressures within the functioning conduits) thereby promoting a faster dissolution of the gas bubble (Konrad & Roth-Nebelsick, 2003). This ameliorating effect appears to be supported by other arguments based on geometric considerations of bordered pit structure during refilling discussed elsewhere (Zwieniecki & Holbrook, 2000; Holbrook & Zwieniecki, 1999).

Moving from bubble to xylem network hydraulics:

The previous analysis considered the 'catastrophe' of an isolated bubble using two control variables: the background liquid pressure in a xylem conduit and initial number of air molecules in an isolated bubble. The necessary conditions for a bubble to become 'unstable' were then established. Unstable bubbles 'fill' a vessel member with air but the 'ease' over which air can be transmitted from an embolized vessel member to another functional vessel remains a topic of active research. The current hypothesis is, as noted earlier, 'air seeding' (Zimmermann, 1983), where the water tension in the functional vessel is sufficiently large to overcome the membrane (or collection of pit-fields) separating the two vessels and thus 'suck' air molecules from the cavitated vessel into the intact vessel (Figure 1a).

The ease of air seeding and subsequent embolism spread is encoded in the xylem vulnerability curve (VC; Fig. 3). Vulnerability of xylem to embolism is expressed by VC that depicts the accumulating loss of hydraulic conductivity (or the percentage loss of conductivity exhibited) relative to the minimum p_s experienced by the sample. Without theoretical VCs, most plant-scale hydraulic models use empirical formulations (Sperry & Tyree, 1988) with the exponential-sigmoid function being the most popular due to its simplicity and to its analytical tractability allowing statistical comparisons of its coefficients (Pammenter & Vander Willigen, 1998). The VC fit to data allows determining coefficients that have a physiological significance and that can be compared among species and plant parts such as, ψ_{50}, which represents the xylem pressure causing 50% loss of the initial hydraulic conductivity (Ogle et al., 2009). In addition, the end of the initial flat zone of those sigmoidal VCs can be interpreted as "air entry point" and represents the xylem pressure causing 12% loss of the initial hydraulic conductivity (ψ_{12} ; Domec & Gartner 2001; Meinzer et al., 2009). The extension of the initial flat zone and the steepness of the VCs depends on interconnectivity and pit membrane resistance to cavitation as derived from the Young-Laplace equation (Mrad et al., 2018, 2021; Roth‐Nebelsick, 2019). Those fitted empirical curves are useful to characterize vulnerability to embolism of a given sample by deriving xylem pressure benchmarks, but on a theoretical point of view the vulnerability of a xylem network can be described from the occurrence of unstable bubbles. Thus, in a network of inter-connected vessels, it is convenient to classify these vessels in a binary manner: embolized (and hence hydraulically dysfunctional) and intact (and hence able to transmit water at maximum hydraulic capacity). In the derivation of VC, the overall xylem tension (or air pressure) is increased gradually in time. As the xylem tension is increased, it is convenient to define the probability of finding an embolized vessel as k_n (hydraulically non-

functional) and thus the probability of finding an intact vessel is $1 - k_n$. The overall hydraulic conductivity of the entire xylem system at that xylem tension (or air pressure) is assumed to be proportional to $1 - k_n$. For embolism to spread in this idealized network due to gradual increases in xylem tension, it is necessary for an embolized vessel to be adjacent to a water filled one (Meyra et al., 2011). In its most elementary form, this argument leads to the following '*self-limiting*' embolism spread

$$\frac{dk_n}{dt} = \frac{dk_n}{dx}\frac{dx}{dt} = b'\, k_n(1 - k_n),$$

where $x = \psi/\psi_o$ is a normalized xylem tension referenced to some xylem tension ψ_o (to be specified later), ψ is the overall xylem tension, $k_n(1 - k_n)$ represent the interaction between a dysfunctional and intact vessel, b' measures how easily an impaired vessel embolizes a water-filled one, and $dx/dt > 0$ is the imposed gradual increase in xylem tension with time during the determination of the VC. Thus, b' encodes all the network information about pit-membranes and the network connectivity among vessel members (this coefficient was set to unity in the work of Meyra et al., 2011). This equation describing the vulnerability of the xylem network with increased time (or air pressure) due to the occurrence of unstable bubbles has two equilibrium points: $k_n = 0$ (no embolism) and $1 - k_n = 0$ (completely dysfunctional hydraulically). Stability analysis shows that $k_n = 0$ (no embolism) is an unstable equilibrium whereas $k_n = 1$ is a stable equilibrium.

Because $dx/dt > 0$ is externally specified and because the goal is to determine the overall hydraulic conductivity of the xylem with respect to increased xylem tension (i.e. VC), the analysis is now focused on the functional relation between variations in k_n and x, an idea originally proposed by Meyra et al. (2011) and is given by

$$PLC = \frac{dk_n}{dx} = b\, k_n(1 - k_n),$$

where $b = b'/(dx/dt)$. The solution of this equation yields a logistic vulnerability curve or percent loss of conductance (PLC) for x >0 given by

$$PLC = k_n = 1 - \frac{1}{1 + exp[b\, x - c_1]},$$

where c_1 is an integration constant. Clearly, this solution does not result in a $k_n = 0$ when $x = 0$ because the exponential term is always positive. This is consistent with the fact that one xylem conduit must be 'infected' with air molecules and experience unstable bubble growth before air seeding can be initiated in the entire xylem network (i.e. $k_n > 0$ for $x \geq 0$ when $dx/dt > 0$). It is possible to mathematically enforce the conditions that at $x = 1$, $k_n = 1/2$ (so that $\psi_o = \psi_{50}$) and that asymptotically $k_n \to 0$ for $x \to 0^+$ (i.e. approached from the positive tension side), the VC can now be expressed as a single parameter curve

$$PLC(x) = \frac{1}{1 + \frac{\exp(b) - 1}{\exp(bx) - 1}},$$

where the coefficient b measures the ease with which embolism spreads by air seeding (though at least one xylem conduit must have experienced unstable bubble growth and hydraulic impairment). In fact, embolism spread in the xylem and disease spread within a susceptible population share many similarities and have been used to explain rich varieties of *PLC(x)* shapes (Roth-Nebelsick, 2019) further discussed in Box 2.

BOX 2: stability analysis, r-shaped and s-shaped VC curves:

Stability analysis: The spread of embolism is given by the dynamical system

$$\frac{dk_n}{dt} = \frac{dk_n}{dx}\frac{dx}{dt} = b' k_n(1 - k_n) = f(k_n),$$

where $b' > 0$ is a control parameter. In this interpretation, it is assumed that x gradually increases in time. The two equilibrium states determined from $dk_n/dt = 0$ or $dk_n/dx = 0$ are $k_n = 0$ (no dysfunctional conduits) and $(1 - k_n) = 0$ or $k_n = 1$ (all conduits are dysfunctional). As discussed in Box 1, the stability of these two equilibrium points can be assessed by evaluating $f'(k_n) = df(k_n)/dk_n = b'(1 - 2k_n)$.

At $k_n = 0$, $f'(k_n) = b' > 0$ (unstable) whereas at $k_n = 1$, $f'(k_n) = -b' < 0$ (stable).

r-shaped and s-shaped VC: To ascertain whether certain VC shapes are prohibited, it is instructive to determine $d(PLC)/dx$ in the vicinity of $x \to 0$ and $x \to \infty$. In the proposed VC logistic model given by

$$PLC(x) = \frac{1}{1 + \frac{\exp(b) - 1}{\exp(bx) - 1}},$$

$$\left.\frac{dPLC}{dx}\right|_{x=0} = \left.\frac{b\exp(bx)\,(\exp(b) - 1)}{[\exp(b) - 2 + \exp(bx)]^2}\right|_{x=0} = \frac{b}{|\exp(b) - 1|} > 0.$$

However,

$$\left.\frac{dPLC}{dx}\right|_{x\to\infty} = \left.\frac{b\exp(bx)\,(\exp(b) - 1)}{[\exp(b) - 2 + \exp(bx)]^2}\right|_{x=0} \to 0.$$

The analysis agrees with the fact that the equilibrium point $k_n = 0$ corresponding to $x = 0$ is an unstable equilibrium whereas the equilibrium point $k_n = 1$ corresponding to $x \to \infty$ is a stable equilibrium. It is to be noted that a $k_n = 0$ at $x = 0$ would have yielded

$$\left.\frac{dPLC}{dx}\right|_{x=0} = b\, k_n(1 - k_n) = 0.$$

However, this dynamical system describes embolism *spread* by air seeding and assumes that at least one vessel member ($k_n > 0$) must have been embolized (formation of unstable bubbles) so that air is 'sucked' from hydraulically dysfunctional vessels into functional vessels.

It can be shown that the maximum inflection point determined from $d^2PLC/dx^2 = 0$ occurs at normalized xylem tensions given by

$$x = \frac{1}{b} log[\exp(b) - 2].$$

For very large b, this inflection point is approximated by $x = 1$ (or $\psi = \psi_{50}$) and the *PLC* appears to be s-shaped and symmetric. However, for $\exp(b) - 2 = 1$ or $b = \log(3)$, $x \approx 0$ and the PLC begins to resemble an 'r-shaped' function. For $b < \log(3)$, the inflection does not exist altogether, and r-shaped functions now dominate the VC (Figure). Likewise, for the Weibull distributed *PLC*, a threshold on d can be formulated when evaluating $d^2PLC/dx^2 = 0$ to yield

$$x \approx (1.443)^{\frac{1}{d}} \left[\frac{1-d}{d}\right]^{\frac{1}{d}}.$$

Hence, $d \to 1$, the inflection point in the PLC occurs near the origin $x \to 0$ regardless of c though $c = (0.693)^{-1/d}$ is selected here to ensure *PLC*=0.5 when $x = 1$. Hence, the existence of an inflection point suffices to assess whether an r-shaped or s-shaped VC exist. In both cases, this inflection point is determined from a single parameter (b for the logistic, d for the Weibull).

An illustration of measured s-shaped and r-shaped VCs are presented in the Figure for two species: *Liriodendron tulipifera* (*Litu)* and *Liquidambar styraciflua* (*List*). The sites, data collection, and method of analysis are described elsewhere (Johnson et al. 2016). The normalized VCs are shown for root, trunk, and branches only. The data suggest that the logistic function reasonably describes all the measured VCs (r- and s- shaped). The normalized VCs for trunk and branch are similar across these two species with minor differences in their b value. The root VC for *List* is r-shaped with no measurable inflection point for $x \geq 0$. For *Litu*, the root VC remains approximately s-shaped and this is confirmed by $d^2PLC/dx^2 = 0$ being found at $x = b^{-1}\, log[\exp(b) - 2] \approx 0.8$. For the trunk and branch VCs, an inflection point exists at $x \approx 1$.

Symmetry and symmetry breaking in VC:

As earlier noted, small b values result in a logistic function becoming approximately 'r-shaped' thereby breaking the symmetry inherent to symmetric sigmoidal functions often used to approximate VCs. However, for large *b*, the s-shaped is maintained along with the symmetry associated with it. It is thus desirable to use the PLC curve and its gradient at x=1 to estimate an 'air-entry' tension and tension at which runaway cavitation occurs in the xylem system. For the latter, it is assumed that the stable equilibrium of 100% loss of conductance is roughly reached by this extrapolation. To do so, the gradient of the PLC at x=1 is first computed to determine these two limiting pressures. For the proposed logistic curve here,

$$\left.\frac{dPLC}{dx}\right|_{x=1} = \frac{b \exp(b)}{4(\exp(b) - 1)},$$

and only varies with b. The associated PLC extrapolated linearly to any normalized pressure is given by

$$PLC_{lin}(x) = \frac{b\exp(b)}{4(\exp(b)-1)}(x-1) + \frac{1}{2}.$$

Hence, the extrapolated pressure at which $PLC_{lin}(x) = 0$ (air-entry) is

$$x = 1 - \frac{2}{b}[1 - \exp(-b)],$$

and at which $PLC_{lin}(x) = 1$ (runaway cavitation) is

$$x = 1 + \frac{2}{b}[1 - \exp(-b)].$$

These two 'end-points' along with $PLC_{lin}(x)$ are also featured in the Fig. B2 for the logistic function at $b = 5$. In practice, the value of b can be determined in a number of ways, including a numerical value of the gradient of the PLC at x=1 or fitting the entire PLC via non-linear regression.

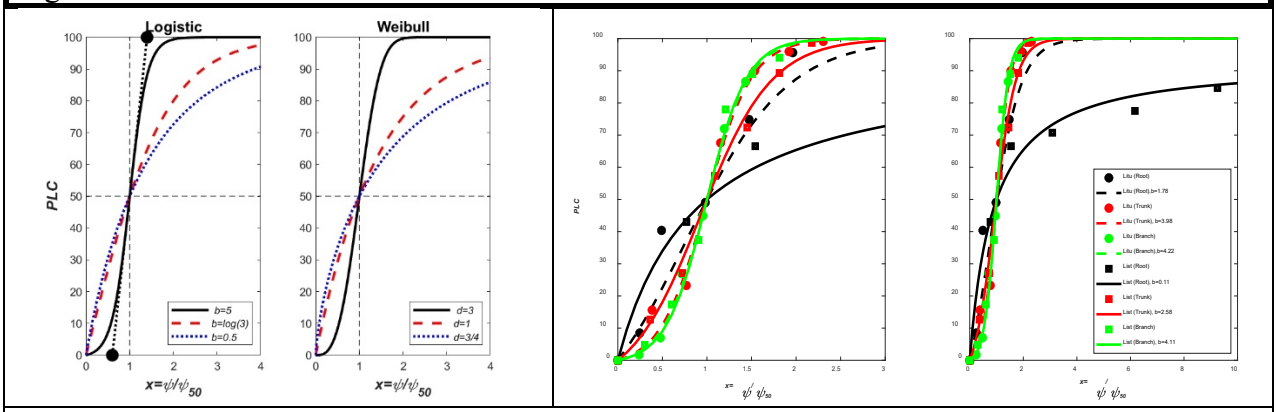

Figure B2: **Left panel**: Illustration of how r-shaped and s-shaped PLC curves emerge from the simplified logistic (left) and Weibull (right) models for embolism spread with constant b (left) and constant d (right). For $b \leq \log(3)$, the logistic *PLC* resembles an r-shaped function whereas for $b > \log(3)$, the *PLC* is s-shaped. Likewise, for $d \leq 1$, the PLC resembles an r-shaped function whereas for $d > 1$, the *PLC* is s-shaped. The two closed circles (left panel) is the extrapolation of the line $PLC_{lin}(x)$ to *PLC*=0 and *PLC*=1 and the determination of their normalized tension x from b only.
Right panels: The organ specific VC for two species - *Litu* and *List* for normalized tension. The branch and trunk VCs are s-shaped and similar (left) whereas the root VC for *List* is r-shaped (right). The left plot is shown over a restricted range of x to illustrate the collapse of branch and trunk level VCs for the logistic curve whereas the right plot is intended to illustrate the r-shaped VC of roots for *List*.

A more complicated network model that considers embolism adjacency and membrane porosity for each pit field can be used to refine the estimate of b. When membrane porosity in each pit-field is represented by a distribution of maximum pore sizes and depend on x (i.e. when the membrane stretches, the pores along the membrane become larger) a non-constant b emerges given by an extreme value distribution

$$b\,k_n = \frac{d}{c}\left(\frac{x}{c}\right)^{d-1},$$

where c reflects the median pressure necessary for air entry into the biggest pores of the population of pit-fields and d is related to the coefficient of variation of these maximum and thus

leakier pores in the aforementioned population of pit-fields (i.e. *the rare pit hypothesis*, Christman et al., 2009).

Inserting this estimate into the simplified embolism spread model yields

$$PLC = k_n = 1 - exp\left[-\left(\frac{x}{c}\right)^d\right],$$

where $c = (0.693)^{-1/d}$ when normalizing a $PLC = 0.5$ at $x = 1$. For $d > 1$, an s-shape vulnerability curve emerges whereas for $d < 1$, an r-shape vulnerability curve emerges (see Box 2). Comparisons for *PLC* shapes for logistic and Weibull are discussed in Box 2.

Xylem hydraulics and the safety-efficiency tradeoff:

Plants have evolved a variety of strategies to prevent hydraulic failure in their conductive tissues while ensuring efficient water delivery to leaves. This hypothesis frames the '*safety-efficiency tradeoff*' or 'runaway embolism' vs 'hydraulic sufficiency' (Tyree & Sperry, 1989). This is the leading hypothesis that seeks to explain why multiple VC shapes exist across different species and why species from different habitats can have such different VCs. Fig. 4 shows the measured VCs for three different species – two desert shrubs and one riparian tree (Sperry, 2000). Clearly, the magnitude of ψ_{50} is large for the desert shrubs and small for the riparian tree. When normalizing these measured PLC with ψ_{50}, the VCs roughly collapse on a single curve, and remaining differences between VCs can be captured by the ease of cavitation spread parameter *b*. The reported maximum conductance for the riparian tree is much larger than the desert shrub. This is the essence of the safety (i.e. ψ_{50}) versus efficiency (maximum conductance) tradeoff.

To illustrate the basic premise behind such tradeoff, whole plant-scale assessment is required. It is thus assumed that the vulnerability curve (logistic or Weibull) represents the root-xylem hydraulic conductivity. Transpiration T_r, which measures the hydraulic capacity of the xylem to deliver water to satisfy the carbon demand of the plant for a preset leaf ψ_l and root ψ_r tension is given by

$$T_r = \frac{1}{h}\int_{\psi_r}^{\psi_l} K(\psi)d\psi,$$

where *h* is the path length from root to leaf (surrogated to plant height). After some algebra and some approximations (see Box 3), it can be shown that the maximum transpiration is given by

$$T_r \approx \frac{K_{max}}{h}\psi_{50},$$

where K_{max} is the maximum hydraulic conductivity of the xylem. Because K_{max} is a measure of maximum hydraulic capacity (efficiency) and ψ_{50} is a measure of safety against cavitation, the safety-efficiency tradeoff emerges naturally from plant hydraulics. In this derivation, it was assumed that $|\psi_r/\psi_{50}| << 1$, $|\psi_l/\psi_{50}| >> 1$ and $b >> 1$.

BOX 3: Maximum transpiration, safety-efficiency tradeoff, and hydraulic segmentation

Maximum transpiration: In the derivation of maximum transpiration here, the VC is assumed to be a logistic function set by its approximate form

$$\frac{K(\psi)}{K_{max}} = \frac{1}{1 + exp[b\ (x-1)]},$$

where $x = \psi/\psi_{50}$ and the interpretation of b is as before. This function captures much of the non-linearities expected in the Weibull shaped VC (see Box 2) but permits analytical tractability without resorting to any special mathematical functions.

As noted earlier, $K(0)/K_{max}$<1 in this VC representation due to the need for a finite number of cavitated vessels to initiate embolism spread by air seeding. With this approximated VC, the transpiration T_r can be expressed as

$$T_r = \frac{1}{h}\int_{\psi_r}^{\psi_l} K(\psi)d\psi = \frac{K_{max}}{h}\psi_{50}\left[\frac{\psi_l - \psi_r}{\psi_o} + \frac{1}{b}log\left(\frac{1 + e^{b\ (\psi_r/\psi_{50}-1)}}{1 + e^{b(\psi_l/\psi_{50}-1)}}\right)\right].$$

To further simplify, let $|\psi_r/\psi_{50}| << 1$ so that

$$T_r = \frac{K_{max}}{h}\psi_{50}\left[\frac{\psi_l}{\psi_{50}} + \frac{1}{b}log\left(\frac{1 + e^{-b}}{1 + e^{b(\psi_l/\psi_{50}-1)}}\right)\right].$$

***Safety-efficiency tradeoff*:** When $|\psi_l/\psi_{50}| >> 1$ and $b >> 1$, then T_r attains only an asymptotical maximum given by

$$T_r = \frac{K_{max}}{h}\psi_{50}\left[\frac{\psi_l}{\psi_{50}} + \frac{1}{b}log\left(e^{-b(\psi_l/\psi_{50}-1)}\right)\right] = \frac{K_{max}}{h}\psi_{50}.$$

This limit shows the origin of the so-called 'safety-efficiency' tradeoff between maximum conductance (K_{max}) and a measure of resistance to cavitation ψ_{50}. This tradeoff appears to be independent of b but only in the limit when $|\psi_l/\psi_{50}| >> 1, b >> 1$ (s-shaped VC). Sperry (2000) showed that T_r attains an asymptotic maximum with increasing ψ_l and that $\partial T_r/\partial\psi_l > 0$ at all leaf tensions. This result is now contrasted to an alternative finding by Manzoni et al. (2013) based on hydraulic segmentation.

***Hydraulic segmentation*:** The hydraulic segmentation vulnerability hypothesis suggests that distal portions of the plant (e.g. leaves) should be more vulnerable to embolism than trunks. The original argument was based on carbon economy of the plant and implies that non-redundant organs (e.g. trunks) require a massive carbon investment when compared to leaves (Zimmermann, 1983). A hydraulic (instead of a carbon investment) explanation can also be offered based on the stability analysis of embryonic bubbles. The stability of embryonic bubbles is linked to background xylem tension as earlier discussed. The higher the background xylem tension, the more unstable the bubbles are and the more prone they are to explosion and embolizing vessels. Based on cohesion-tension theory, this tension is largest next to leaves – at least when compared to the trunk, and this is the idea behind the original hydraulic segmentation hypothesis (Zimmermann, 1983). The immediate consequences of this result is that leaf xylem tension may be limiting the operating pressure of the xylem. Some evidence across many species has been offered (Tyree et al., 1993; Tsuda & Tyree, 1997; Johnson et al., 2016).

Using this interpretation, Manzoni et al. (2013) considered the maximum transpiration estimate with the limiting approximation $K(\psi)\sim K(\psi_l)$ so that

$$T_r = \frac{1}{h}\int_{\psi_r}^{\psi_l} K(\psi)d\psi \sim K(\psi_l)\left(\frac{\psi_l - \psi_r}{h}\right),$$

where the symbol '~' indicates scales as or proportional to. Using the same logistic function with $x = \psi_l/\psi_{50}$ and upon ignoring root tension compared to leaf tension, T_r reduces to

$$T_r = \frac{K(\psi_l)}{h}\psi_l = \frac{K_{max}\psi_{50}}{h}\frac{x}{1 + exp[b\ (x-1)]}.$$

As ψ_l increases, the (linear) driving force for transpiration increases but the nonlinear $K(\psi_l)$ decreases. Manzoni et al. (2013) demonstrated that a maximum transpiration must then exit and can be determined from

$$\frac{\partial T_r}{\partial \psi_l} = 0 = \frac{K_{max}}{h}\psi_{50}\frac{[1 + (1 - b\,x)\,\exp(b(x-1))\,]}{[1 + \exp(b(x-1))]^2} = 0.$$

A solution of this algebraic equation for x can be expressed in closed form as

$$x_m = \frac{\psi_l}{\psi_{50}} = \frac{1 + \boldsymbol{W}[\exp(b-1)]}{b},$$

Where $\boldsymbol{W}[.]$ is the Productlog or the principal Lambert W-function that arises frequently in mathematical solutions of the susceptible-infectious-recovery or SIR model in epidemiology as recently reviewed elsewhere (Katul et al., 2020). Its value is given by the alternating series

$$\boldsymbol{W}[\boldsymbol{u}] = u - u^2 + \frac{3}{2}u^3 - \frac{8}{4}u^4 + \frac{125}{24}u^5 - \cdots.$$

and the corresponding maximum transpiration at x_m is given by

$$T_r = \frac{K(\psi_l)}{h}\psi_l = \frac{K_{max}\psi_{50}}{h}\zeta(b); \zeta(b) = \left\{\frac{x_m}{1 + exp[b\ (x_m - 1)]}\right\}.$$

A comparison of the two transpiration solutions, the continuous distribution of tension versus tension set by the most distal organ – the leaf, is featured in Figure.

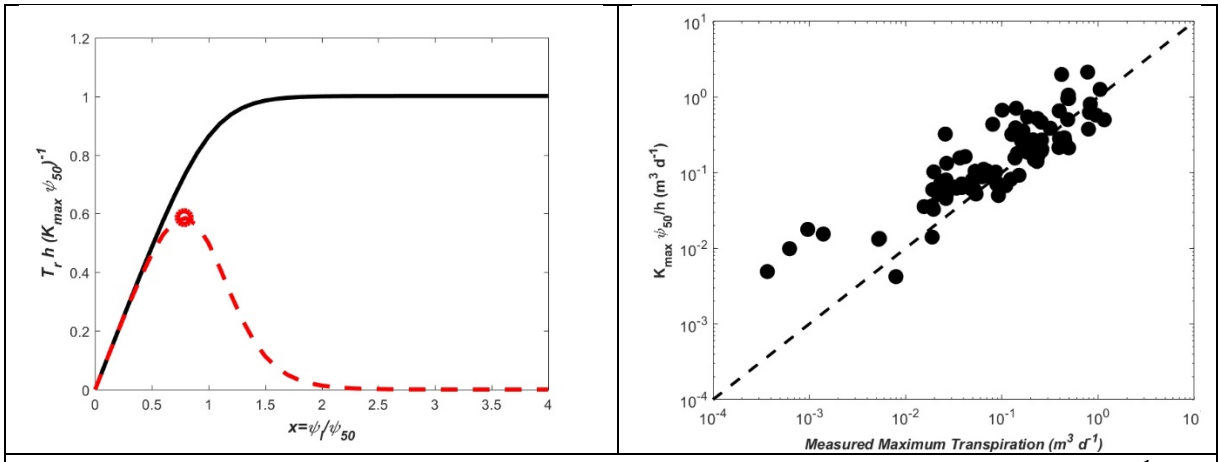

Figure B3: **Left panel**: comparison between normalized transpiration $T_r\ h\ (K_{max}\psi_{50})^{-1}$ against normalized leaf tension $x = \psi_l/\psi_{50}$ for the continuous tension distribution across the entire root-xylem system (black solid) and the hydraulic segmentation limit where leaf tension dominates the entire hydraulic conductivity (red dashed). The same vulnerability

curve is used in both calculations ($b = 5$). In the latter case, a clear maximum transpiration emerges (open circle) at $x_m$whereas in the continuous xylem tension case, it does not. **Right panel**: comparison between measured and modeled maximum transpiration (=$K_{max}\ \psi_{50}h^{-1}$) over 3 orders of magnitude. The one-to-one line is also shown (dashed). The analysis is suggestive that a safety-efficiency tradeoff can emerge between K_{max} and $\psi_{50}h^{-1}$(i.e. a hydraulic gradient) when conditioned on maximum transpiration. The data set includes the following: *Acer saccharum, Betula papyrifera, Carapa procera, Cecropia longipes, Eucalyptus grandis, Eucalyptus regnans, Eucalyptus saligna, Fagus sylvatica, Larix cajanderi, Larix gmelinii, Liquidambar styraciflua, Liriodendron tulipifera, Picea mariana, Pinus banksiana, Pinus pinaster, Pinus radiata, Populus tremuloides Populus Sp,, Pseudotsuga menziesii, Salix matsudana, Quercus alba, Quercus rubra,* and *Quercus petraea.*

Unsurprisingly, the hydraulic segmentation argument yields a lower maximum transpiration due the fact that ψ_l restricts water transport across the entire xylem (Fig. B3). This reduction from the maximum predicted by the continuous description is captured by $\zeta(b) < 1$. More significant is that the two solutions differ fundamentally in how they predict normalized transpiration to vary with normalized leaf tension. In the hydraulic segmentation limit, $\partial T_r/\partial\psi_l = 0$ exists at a unique leaf tension x_m whereas in the continuous xylem tension case, it does not. Hence, the continuity of xylem tension and its variability within the plant must be accommodated in hydraulic representation of the soil-plant system. A logical follow-up question to ask is how well $K_{max}\ \psi_{50}h^{-1}$ recovers maximum transpiration in trees. The data set used in Manzoni et al. (2013) is revisited and comparisons between reported and predicted maximum transpiration from $K_{max}\ \psi_{50}h^{-1}$is shown in Fig. B3. Given that the plant hydraulic traits and the maximum transpiration were not even measured at the same geographic locations, agreement between measured and predicted maximum transpiration rates in the figure can be deemed acceptable.

403

404 The link to the VBE and other climatic factors can now be made explicit when noting that

405 $$P_g = WUE\ \frac{Tr}{L} = \left[1.6\ \frac{c_a}{VPD}\left(1 - \frac{c_i}{c_a}\right)\right]\frac{K_{max}}{h\,L}\psi_{50}\left[\frac{\psi_l}{\psi_{50}} + \frac{1}{b}log\left(e^{-b(\psi_l/\psi_{50}-1)}\right)\right],$$

406 where $WUE$is the leaf-scale water use efficiency, $c_a$and c_i are atmospheric and intercellular CO_2
407 concentrations, respectively, VPD is the vapor pressure deficit that depends on the saturation
408 vapor pressure (and thus temperature) and relative humidity in the atmosphere, and L is as
409 before the leaf area. Numerous theories, including those based on stomatal optimization,
410 reasonably predicted WUE from the aforementioned drivers (e.g. Katul et al., 2010).

411

BOX 4: Embolism and cell wall mechanics shift the fold to cusp catastrophes

Large bubbles in an embolism vessel or tracheid are influenced by cell wall mechanics and pit membrane properties. The mathematical description of such interactions between cell walls and bubbles remains fraught with difficulties though catastrophe theory can make qualitative and general statements about such interaction. For simplicity, the case where pits rapidly close so as to isolate an intact from an embolized tracheid is considered for illustration. Such pits approximate the torus margo in conifers. It is shown here that the inclusion of cell wall

mechanics switches the previously studied catastrophe in bubbles from 'fold' to 'cusp'. The cusp catastrophe has a long tradition in mathematical ecology and was first employed to explain the repeated outbreak of the spruce budworm in forests (Ludwig et al., 1978).

As before, the xylem liquid pressure p_s before embolism occurs is assumed to be the same for two adjacent intact tracheids. After embolism commences in one of them (due to air seeding), p_s is assumed to represent the intact tracheid pressure only. A large and saturated bubble of radius R carrying n air and water vapor molecules is now considered. For large bubbles, the liquid pressure in an isolated embolized tracheid must increase or liquid tension must be reduced because water molecules are being pushed together in the now sealed tracheid. The contracting force acting on this large bubble of surface area (=$4\pi R^2$) is only surface tension whereas the expanding forces are, as before, xylem pressure p (negative) and the gas pressure within the bubble. At equilibrium, a force balance between contracting and expanding forces reduces to (Konrad & Roth-Nebelsick, 2006)

$$8\pi\gamma R + 4\pi R^2 p - \frac{3\Re\, T\, n}{R} = 0,$$

where the first, second, and third terms represent the surface tension, xylem pressure p, and gas pressure due to air and water vapor molecules. When $p = p_s$, the analysis reduces to the one earlier described with the assumption that no pressure differential exists to close the pit membrane between intact and embolized vessel. This case is labeled as the 'small-bubble' scenario because the bubble volume is presumed to be sufficiently small compared to the vessel volume so as not to impact the background xylem pressure. It leads to the fold catastrophe earlier mentioned in Figure 2. For larger bubbles, deviations between $p(> p_s)$ and p_s occur and are thus responsible for rapidly closing the pit membrane ensuring hydraulic isolation between embolized and intact tracheid. To proceed further and bring into focus a connection between cell wall mechanics and embolism, a relation between p and p_s is required within the embolized tracheid. A simplified version of the approach in Konrad & Roth-Nebelsick (2006) is now followed to arrive at this relation. In this revised approach, water is assumed to be incompressible, the cell walls are assumed to be elastic, and the expanded bubble volume must be accompanied by an expansion in tracheid volume. Defining the undeformed tracheid volume as V_o, the change in tracheid volume due to the presence of large bubbles as $\Delta V = (4/3)\ \pi R^3$, and the cell-wall material compressibility μ as

$$\mu = \frac{\Delta V}{V_o}\frac{1}{p - p_s},$$

the xylem pressure is now

$$p - p_s = \frac{1}{\mu}\frac{1}{V_o}\frac{4}{3}\pi R^3.$$

The p_s represents both the liquid pressure prior to embolism and the liquid pressure in the intact tracheid. Once $|p - p_s|$ exceeds a small threshold (or the bubble size exceeds a threshold), the torus margo membrane closes and ensures hydraulic isolation (Schulte and Hacke 2021). Beyond this point, the torus margo membrane is assumed to remain intact. Inserting this result into the force balance at equilibrium leads to

$$8\pi\gamma R + 4\pi R^2\left[p_s + \frac{1}{\mu}\frac{1}{V_o}\frac{4}{3}\pi R^3\right] - \frac{3\Re\, T\, n}{R} = 0.$$

This equation can be re-arranged as a sextic (order 6) polynomial in bubble radius R that is given by

$$\left[\frac{1}{\mu}\frac{1}{V_o}\frac{16}{3}\pi^2\right]R^5 + 4\pi p_s R^2 + 8\pi\gamma R - \frac{3\Re\, T\, n}{R} = 0.$$

There are no exact solutions for such a polynomial equation. Konrad & Roth-Nebelsick (2006) considered 'asymptotic' cases and showed that for large R, the last two terms in the force balance can be ignored leading to

$$\frac{R}{{V_o}^{1/3}} = \left[\frac{-3}{4\pi}p_s\mu\right]^{1/3}.$$

This dimensionless 'large radius' equilibrium is stable and independent of surface tension and number of air molecules. It only depends on the xylem tension prior to embolism and cell wall compressibility. To link μ to common material properties, the tracheid is assumed to be cylindrical with wall thickness d_t, undeformed radius r_t and length l_t, with a Poisson number σ_t and Young's modulus of elasticity E_t. In this case, Konrad & Roth-Nebelsick (2006) showed that μ depends on the structural and undeformed geometric properties of the tracheid and is given by

$$\mu = \left(\frac{2r_t}{d_t}\right)\left[\frac{1-(\sigma_t)^2}{E_t}\right].$$

It is noted that R scales as $\mu^{1/3}$, which makes R insensitive to small variations in E_t or σ_t. When $V_o = \pi {r_t}^2 l_t$, the relation between the tracheid and large bubble radius is given by

$$\frac{R}{r_t} = \left\{\frac{-3}{2}p_s\left(\frac{l_t}{d_t}\right)\left[\frac{1-(\sigma_t)^2}{E_t}\right]\right\}^{1/3}.$$

For a coniferous tracheid with $\sigma_t = 0.5$, E_t=10^4MPa, $l_t/d_t = 4\times10^3$, and $p_s = -1$ MPa, R/r_t=0.77. An E_t= 8 - 10GPa has been reported for cell walls for *Albizia julibrissin*, *Acer negundo*, and *Pinus taeda* (Domec et al., unpublished data). The E_t for the torus margo membrane (compared to cell walls), which constitutes only a small fraction of the tracheid surface area, are an order of magnitude smaller ranging from 0.4-0.9 GPa (and their effects are ignored). The analysis here suggests that the bubble radius expands to a maximum of 0.77 the tracheid radius, and thus embolism does not entirely replace the water with air. The trapped water within the isolated tracheid can thus play an under-appreciated role in bubble dissolution (unless the torus margo membrane fails because of structural fatigue or large pressure differential across it).

Returning to the small R case, the first term in the force balance can be ignored thereby recovering the previous findings about bubble dynamics. That is, the force balance is now governed by the cubical equation

$$4\pi p_s R^2 + 8\pi\gamma R - \frac{3\Re\, T\, n}{R} = 0.$$

Two positive real roots only exist when $n < n_{max}$, where n_{max} is given as before

$$n_{max} = \frac{2\pi\gamma}{\Re\, T}\left(\frac{8\gamma}{9p_s}\right)^2.$$

The two roots correspond to one unstable and one stable equilibrium (i.e. a fold catastrophe). The bifurcation diagram with respect to the two control variables p_s and n is featured in Fig. B4. The existence of an unstable branch between two otherwise stable equilibrium radii is indicative of a hysteretic behavior in bubble dynamics (expansion and dissolution) when the control variables change.

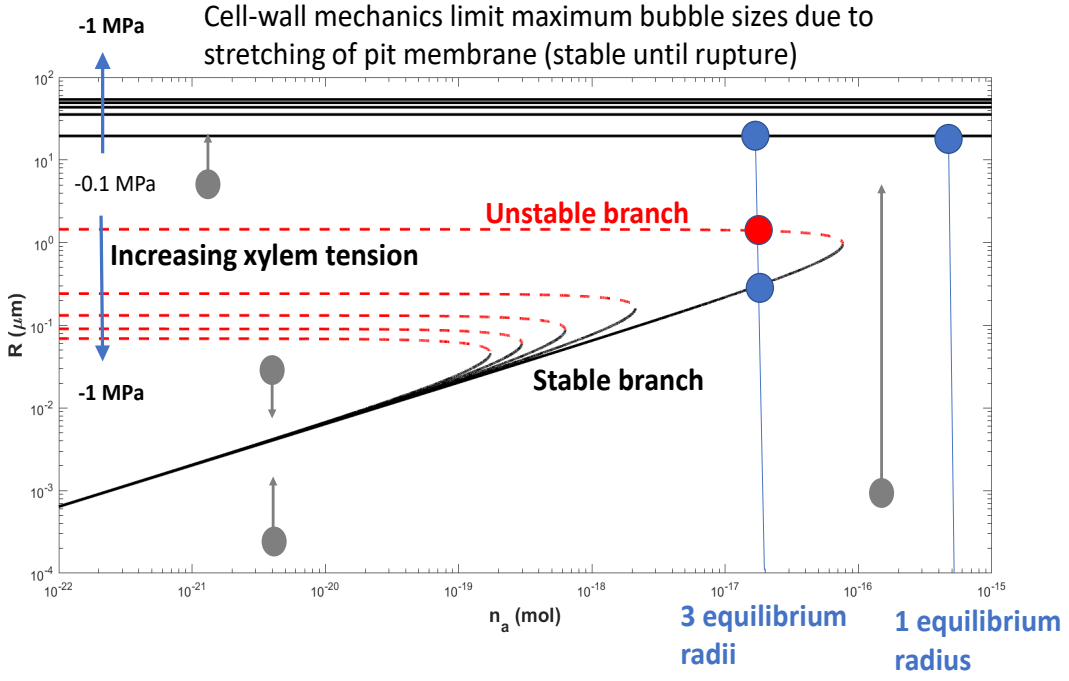

Figure B4: Bifurcation diagram shown in two-dimensions (equilibrium R versus n) with variations in p_s shown as multiple curves instead of a separate dimension illustrating the genesis of a cusp catastrophe. The link between the unstable branches (red dashed line) and the stable large bubble size branch (horizontal lines) needed to complete the surface (and cusp) is not shown though it can be computed numerically. The dynamical system always exhibits at least one stable equilibrium (the large radius case – shown as horizontal lines). The remaining two equilibria only exist for $n < n_{max}$, where n_{max} decreases with increasing p_s.

A survey of underlying mechanisms generating catastrophes in plant hydraulics

To bridge the bubble-scale to whole-plant hydraulic failure, the mechanisms leading to the non-linearities in the vulnerability curves across various organs and their upscaling to whole tree must be understood. Here, the most relevant discoveries to plant hydraulic failure at different scales are summarized and areas where general understanding is lacking are highlighted.

Pits – structure and function

Maximum pore size in pit membranes should be the primary determinant of air-seedling in angiosperms (Zimmerman, 1983; Tyree & Sperry, 1989) and the air-seeding and filling of a

conduit with air is another example of a catastrophe (as in the bubble expansion example, above). Network theories in which air spread within the xylem is based on maximum pit membrane pore size also proved effective in predicting the shape of vulnerability curves (Mrad et al., 2018). According to extreme value theory, selecting the maximum pore of each pit membrane and determining their probability distribution across the entire organ converges to a generalized extreme value distribution of which the Weibull function is a special case. This probability law may offer a plausible explanation why VCs appear to exhibit Weibull shaped properties (Mrad et al., 2018).

However, determining actual pit membrane pores sizes has been elusive. Preparation and imaging of pit membranes is difficult as they are prone to deformation, particularly during drying (Zhang et al., 2017; Kotowska et al., 2020). Recently, Kaack et al. (2021) modeled pore sizes and obtained good agreement between predicted (based on pore sizes) and measured vulnerability curves. Another interesting and potentially important property of pit membranes is their composition: more hydrophobic or hydrophilic polymers in the membrane network may serve to either increase or decrease resistance to air-seeding and rupturing. Novel imaging technologies may be needed to elucidate the structure of pit membranes. For example, the development of new nanometer-scale 3d x-ray microscopy systems may be used to detect the nano-scale pores in these membranes and their distributions throughout the membrane matrix. This will allow determining pathlengths, constrictions (Zhang et al., 2020) and tortuosity of water pathways in xylem pits. Additionally, methods that allow the determination of pit membrane chemical composition and nanomechanical properties will be important for describing both water flow through pits and air-seeding properties (Capron et al., 2014).

The resistance due to water flow through xylem pits is commensurate to the resistance of water flow through xylem conduits in both angiosperms and gymnosperms (Sperry et al., 2005; Pittermann et al., 2006; Sperry et al., 2006). Although in gymnosperms, there does seem to be slightly more resistance in pits than in the conduits themselves (Pittermann et al,. 2006; Domec et al., 2006). Water flow through a regular pit field may be better approximated by the so-called Sampson flow, which relates the flow rate through a thin perforated plate to the pressure drop across the plate (Jensen et al., 2016). In Sampson flow, the resistance depends on the inverse cube of the perforation radius instead of inverse fourth power of the pipe radius as in the Hagen-Poiseuille flow, underscoring the hydraulic significance of large pores within the pit. Sampson flow is one possible approximation when viewing the pit field as a thin sheet with multiple but well separated pores whereas Darcy's law may provide another approximation when viewing water flow through the pit as a low Reynolds number porous medium. What is clear is that understanding of water flow through pit membranes is still in its embryonic state and this is an area where improvements in theory and experiments are needed urgently.

Torus-margo pits common in coniferous species are particularly interesting due to their mechanism of sealing and isolating functional tracheids from embolized tracheids (Hacke et al., 2004; Schulte & Hacke, 2021; Box 4). Recent work has shown that displacement of the torus requires very little pressure difference between two adjacent tracheids: somewhere between <0.1 to 0.5 MPa is required to move the torus from its centered position (Domec et al., 2006; Zelinka et al., 2015) but more pressure may be required to completely seal the torus against the pit wall (Schulte & Hacke, 2021). More research is needed to understand the properties of torus-margo pits and this partial list includes: the pressure differentials required for sealing in different species and organs, the nanomechanical properties such as elastic modulus of the margo

(estimated as 0.012 GPa for *Pinus taeda* from force-displacement curves performed with an atomic force microscopy; Domec et al., unpublished data), the importance of the fit of the torus-chamber seal (sometimes called overlap; Delzon et al., 2010) and how much of current estimates are sensitive to methodological issues (SEM, drying), the occurrence of pores in the torus (Jansen et al., 2012) and its mechanical properties, the permanence of torus aspiration (Comstock & Côté, 1968), and weaking of the margo fibers from repeated stretching (see below).

With regards to structural properties, xylem in certain species can have reductions in embolism resistance over courses of embolism and refilling (Hacke et al., 2001; Feng et al., 2021) and negative pressure cycles (Umebayashi et al., 2019). The underlying mechanism behind "cavitation fatigue" is thought to be structural fatigue of the pit membrane due to stretching (Tixier et al., 2014; Hillabrand et al., 2016). This stretching is a result of pressure differentials across the pit membrane. For example, if an embolized conduit is adjacent to a fully functional one, the pressure in the embolized conduit will be commensurate to atmospheric but water in the functioning conduit will be under tension thus pulling the membrane toward the functional conduit. Multiple cycles of stretching and relaxing may lead to weakened membranes that are more prone to air-seeding. The reduction in embolism resistance due to cavitation fatigue will have hysteretic effects on plant hydraulic function and could lead to runaway cavitation (Sperry et al., 1998) and plant death.

Hydraulic network properties

Although of great interest for decades (see Zimmermann, 1983), hydraulic network topology has proven difficult to measure (but see Zanne et al., 2006; Schenk et al., 2008). Models have been developed to address the topics of the degree of vessel interconnectedness or sectoriality (Loepfe et al., 2007). More recently, Mrad et al. (2018) used pit membrane and vessel properties to develop a network model to successfully upscale to branch-level vulnerability curves in a diffuse porous species. In this model, vessel element and pit resistances are determined using Hagen-Poiseuille and Sampson methods respectively. The model captures pertinent xylem features that allow the manifestation of the 'rare-pit' hypothesis (Christman et al., 2009). Initial embolisms are introduced followed by gradual increase of bubble pressure to induce air-seeding events similar to the air-injection technique. The process goes on until 100% loss of conductivity and a VC is obtained as shown in Fig. 5 and the resulting VC is featured in Fig. 6.

Mrad et al. (2021) extended this model to test the effects of vessel connectivity and found that greater connectivity resulted in reduced embolism spread and also highlighted the large effect that vessel length has on hydraulic conductivity. Hydraulic network properties also have implications for catastrophe like behavior. One question arising from this is "Would a more integrated (more vessel-vessel connections) or a more solitary network topology be more likely to suffer runaway cavitation?" The work of Mrad et al. (2021) suggests that there may be optimal degrees of vessel-vessel integration to prevent catastrophic hydraulic failure.

Much work has been devoted to analysis of xylem conduit diameters and the resulting impacts on hydraulic conductivity (e.g., McCulloh et al., 2010) and their tapering from tree base to tip (Anfodillo et al., 2006; Olson et al., 2021). However, conduit length has an equally large (if not larger) effect on the overall resistance of the xylem system due to minimizing the numbers of pit crossings. Although vessel length distributions are labor intensive, future work can be

directed towards understanding conduit length distributions and their effects on hydraulic transport. Undoubtedly, network topology should include coniferous and ring porous species and the impact of vasicentric tracheids (Carlquist, 1985; Percolla et al., 2021) and vessel relays (Brodersen et al., 2013) on xylem network properties.

Compared to the "superhighway" of dead cells that make up the xylem, the symplastic pathways of hydraulic transport through plants have much greater resistance to water flow. These pathways occur in the leaf (parenchyma) and the root (endodermis) and are likely 6-7 orders of magnitude less conductive than xylem conduits (e.g., Hammond et al., 2021). Potential other symplastic flows could be in parenchymatous tissue in the xylem (e.g., ray parenchyma) or in connecting xylem and phloem (see below). At this point, it is not known whether or not these tissues could serve as failure points for hydraulic transport through entire plants. It appears that aquaporins play a large role in transport through these tissues (Maurel & Prado, 2017; Domec et al., 2021) and if aquaporin activity were reduced to make these tissues even lower in conductivity, then they could become large bottlenecks that could result in plant tipping points for hydraulic failure. There is an undisputed need into exploring the relative conductances of these tissues and how they change with dehydration. Additional research is also needed on the effectiveness of aquaporins in water transport as tissues dehydrate.

Water flow through leaves is an exciting and developing field. Water must be transported apoplastically through the leaf venation system and may also be transported apoplastically along the cell walls of mesophyll tissue before evaporating into intercellular spaces. However, many leaves contain endodermis-like bundle sheaths around the vascular tissue (Lersten, 1997; Liesche et al., 2021; Trueba et al., 2021) that would force water through the symplast of the bundle sheath. Further, the bundle sheath (suberized or not) exerts strong control over whole leaf hydraulic transport and aquaporins appear to be involved in water movement across the bundle sheath (Shatil-Cohen et al., 2011; Moshelion et al., 2015). The pathways of water through leaves are complex and less well-understood than those through xylem but new modeling and imaging developments are expanding the understanding of leaf water transport (Albuquerque et al., 2020; Treuba et al., 2021). One of the largest unknowns in symplastic transport of leaves and roots is knowledge of individual cell water transport properties and how they vary through time but also with species and in different organs.

Arguably, one of the least well-understood water transport pathways in woody plants is the symplastic flow from phloem and inner bark through the cambial region and into the xylem (and the reverse) (Sevanto et al., 2011; Pfautsch et al., 2015). A recent study has shown that if this hydraulic transport pathway fails, this failure could represent a tipping point for tree mortality (Lamacque et al., 2020; Preisler et al., 2021; Hammond et al., 2021). In the study of Preisler et al. (2021), droughted trees that had received drought-ending precipitation either resumed radial water transport to pre-drought levels and survived or did not resume radial water transport and died. The failure of radial water transport happened months before axial (sap flow) transport failed. Similarly, Lamacque et al. (2020) observed that in droughted lavender plants, once a threshold of branch diameter shrinkage had occurred, the plants could no longer rehydrate, suggesting that the phloem and cambial tissues were dead and suppressed radial water flow altogether. Radial water transport between phloem and xylem may be a new target for monitoring the likelihood of trees succumbing to mortality due to drought and drought and

rewatering experiments combining sap flow and dendrometers could be used to determine these thresholds for mortality.

The canopy underground

The xylem network of overlapping conduits extends to the roots where the negative pressure pulls water from the soil (Steudle, 1994). Not surprisingly, root hairs have evolved to allow the plant to take in as much water and minerals from the soil as possible. Whereas leaves maximize carbon gain for a given loss of water (Givnish & Vermeij, 1976; Sperry et al., 2017), roots perform the opposite optimization – maximize water and nutrient uptake for a given investment in carbon for root construction (Guswa, 2008). Water and dissolved minerals from the soil move into the root hairs by osmosis and travel into the xylem found in the root, where they are transported to the rest of the plant. As in the leaves, there is a symplastic and apoplastic water pathway from the root hairs and across the root cortex. Then, at the root endodermis that represents a single layer of cells bordering the cortex, water is forced by reverse osmosis through cell membranes because of the Casparian strip that forms an apoplastic barrier. Under saturated soil and low transpiration, ions accumulate in the root xylem thus allowing water to move into root xylem by osmosis and generating a positive pressure called "root pressure" (Tibbets & Ewers, 2000). Soil water is also usually under a negative pressure because like in plant xylem, capillary forces hold water between soil particles (Fig. 7). Therefore, the cohesion–tension mechanism at the soil-root interface represents also a "tug-of-war on a rope of water" between capillary forces in cell walls and capillary forces in soil. In dry soil, plants have to pull against soil water potentials of −1 MPa or lower. In addition, because of the reverse osmosis at the root, the xylem must extract water not only from the soil pore space, but also against the osmotic strength of the soil solution.

If the loss of soil hydraulic conductivity occurs at water less negative than xylem pressure thresholds, then xylem vulnerability and xylem hydraulic is not the main determinant of transpiration (Sperry et al., 1998; Körner, 2019). Belowground hydraulic failure outside of the xylem was associated with tree mortality during a severe drought in Texas (Johnson et al., 2018). Modeling studies in that and many other systems indicated that the most likely hydraulic failure point was in the rhizosphere (Siqueira et al., 2008; Huang et al., 2017; Mrad et al., 2019). In fact, plants are built to minimize the possibility of belowground hydraulic failure. In loblolly pine trees growing on sand versus loam, xylem vulnerability to embolism was greater on loam even though sand is considered drier (Hacke et al., 2000). But the pines had produced xylem that was representative of the extraction limit for water in each soil type: there is no need to build highly resistant xylem if the soil that the plant is growing in has a high (less negative extraction limit). Having overbuilt xylem in the sand would only lead to hydraulic dysfunction in the rhizosphere.

The hydraulic conductivities of the xylem of the different plant organs (leaves, branches, stem and roots) and of the soil are variable. The radial conductance of the root is also variable and it is affected by root surface area as well as by the expression and activity of aquaporins (Ehlert et al., 2009; Chaumont & Tyerman, 2014). Most of the studies linking stomatal regulation to plant hydraulics focus on xylem vulnerability as the primary constraint on water flow in soil and plants,

neglecting the explicit role of soil hydraulic conductivity but with several exceptions (Siqueira et al., 2008; Manoli et al., 2014, 2017; Huang et al., 2017; Mrad et al., 2019). The question that appears is "What are the primary constraints that regulate stomata and water flow across soil-plant continuum?" An answer to this long-standing question requires methods to measure and partition the hydraulic conductance of the different elements of soil-plant system (Johnson et al., 2016; McCulloh et al., 2019). Water loss at leaves depends on continuous supply of water in the xylem from the soil to absorbing roots (Passioura, 1988), which is often described as analogous to Ohm's and Kirchhoff's laws (Sperry et al. ,1998). Applying these laws to plants, the water flow depends on water potential gradients and the resistance of pathways of soil-plant continuum. Under wet soil conditions, the soil hydraulic conductivity is sufficient to sustain transpiration but in drier soils, the soil can become the limiting factor for water flow into the roots as its hydraulic conductivity decreases below than that of roots (Sperry et al., 1998; Draye et al., 2010; Carminati & Javaux, 2020).

Plant water supply function (transpiration versus leaf or soil water potentials) models now use soil-to-leaf (whole plant) vulnerability curves in concert with the soil-to-leaf hydraulic conductance to water flow (Johnson et al., 2016; Sperry & Love, 2015). In its simplest representation, soil to leaf hydraulic conductance ($K_{\text{soil-leaf}}$) can be viewed as the result of two conductances in series:

$$K_{soil-leaf}(\Psi) = \frac{1}{\frac{1}{K_{soil-root}(\Psi)} + \frac{1}{K_{root-leaf}(\Psi)}},$$

where $K_{\text{soil-root}}$ represents the water-potential-dependent decrease in rhizosphere (i.e. the volume of soil adjacent to the plant roots) conductance (Figure 5), and $K_{\text{root-leaf}}$ is the hydraulic conductance of the whole plant system (i.e. from the roots to the leaves). Each organ axial conductivity (K_{root}, K_{trunk}, K_{branch} and K_{leaf}) constituting $K_{\text{root-leaf}}$ can decrease from its initial conductivity at full saturation to account for the loss of hydraulic conductivity (vulnerability curves; Figures 3 and 4). Further, $K_{\text{soil-root}}$ can be decomposed into two components:

$$K_{soil-root}(\Psi) = \frac{1}{\frac{1}{K_{soil}(\Psi_{\text{soil}})} + \frac{1}{K_{root}(\Psi_{\text{root}})}},$$

where K_{root} represents the radial root conductance and K_{soil} is the effective soil hydraulic conductance characterizing the ease of water flow from the soil to a given surface area of root ($A_{\text{root}} = 2\pi r_{\text{root}} L_{\text{root}}$, where r_{root} is root radius, and L_{root} is root length) defined as (Nobel and Cui 1992)

$$\frac{K_{soil}(\Psi_{\text{soil}})}{K_s(\Psi_{\text{soil}})} = \frac{A_{\text{root}}}{r_{\text{root}} \ln\left(\frac{r_{\text{soil}}}{r_{\text{root}}}\right)}$$

where $K_s(\Psi_{\text{soil}})$ describes the decline in saturated soil hydraulic *conductivity* (K_{sat}; Fig 5) in response to soil water potential away from the root, r_{soil} is the radial distance from the center of the roots to the mean distance between roots (Campbell, 1985; Doussan et al., 1998). Here, it is assumed that each root is a cylinder uniformly spaced and therefore $r_{\text{soil}} = (\pi \text{RLD})^{-1/2}$, where RLD is the root length density (total length of roots per unit of soil volume). Quantifying canopy versus

root effects on plant hydraulic is often conducted by inspecting the ratio of projected leaf area index (LAI) to total root area index (RAI = $2\pi r_{root}$RLD, with r_{root} ranging from 80 to 100 microns for unsuberized fine roots and from 5 to 10 microns for root hairs; Dittmer, 1949). Most water and nutrients are absorbed by roots hairs, cells formed on the epidermis of the region of root maturation. In most angiosperms and some conifers, root hairs often form on fine roots and thus increase their effective absorbing surface area (McCully, 1999). Because root hair diameter and above all root hair length are difficult to determine due to their fragile and unicellular structure, most root area values are based on fine roots and should be replaced by fine root diameter that is typically around 100 microns. The $K_s(\Psi_{soil})$ can be parameterized using several empirical power-law functions relating the rapid decline in K_{sat} as soil moisture or consequently soil water potential declines (Brooks & Corey, 1964; van Genuchten, 1980; Campbell, 1985). When the soil particle size distribution is described by power-laws (i.e. fractal), there is theoretical support for these assumed empirical shapes offered by percolation theory (Hunt, 2005).

Box 5: Comparing xylem and soil conductances: A case study

Applying monotonic declines in predawn water potentials, the conductivity in each organ can then be decreased proportionally to the loss in conductivity observed in their respective VCs (Johnson et al. 2016). This approach requires information on vulnerability to embolism in each plant organ but also the partitioning of the total plant resistance in roots, trunk, branches and leaves. When the trees are fully hydrated, partitioning in roots and leaves represent each 40% of the whole-tree resistance to water flow, respectively. The remaining aboveground hydraulic resistance represented 10% and 10% in trunk and branches, respectively, which reflected the differences in sapwood conductivity usually measured in those two organs (Domec et al., 2009). Soil texture was allowed to vary to represent either a sandy soil, a sandy loam, or a loamy soil. Root density conductance is a factor accounting for the length and geometry of the root system (assumed to represent a cylindrical rhizosphere sheath of 5-mm thickness from bulk soil to root surface) and varied to represent a root to leaf area ratio (RA/LA) of either 1 or 7. Those simulations show the effect of soil texture on $K_{soil\text{-}leaf}$ and the greater influence of RA/LA on $K_{soil\text{-}leaf}$ than vulnerability to embolism (Fig. B5). These data support observations and previous modelling efforts that on sandy soils plants maintain higher hydraulic conductance by exhibiting a higher RA/LA rather than by having a xylem more resistant to embolism, because the higher RA/LA minimizes the development of limiting hydraulic resistances in the soil–root continuum (Sperry et al., 1998; McCulloh et al., 2019; Carminati & Javaux, 2020).

Furthermore, there is no advantage in having more embolism resistant plant organs in environments where soil hydraulic conductance limits water transport (Fig. 7, but also see Sperry et al., 1998; Johnson et al., 2018). Indeed, reducing RA/LA may actually increases the probability of hydraulic failure as soils dry (Teskey et al., 1983), even if plants produce more embolism-resistant xylem (Ewers et al., 2000). Increasing RA/LA from 1 to 7 induced a shift from rhizosphere conductance to xylem loss of conductance (Fig. B6). However, as root to leaf area ratio increased, the rhizosphere became more limiting for sandy soil (switching from -0.5 to -1.5 MPa), and with gradually less of an effect in less porous soils. Therefore, determining not only root area but also soil texture is essential to predict the effect of drought on plant transpiration. In coarse soil, the loss of soil hydraulic conductivity occurs at water potentials less negative than plant xylem Ψ_{50} (set at -3.0 MPa in simulations shown in Fig. B6). In sandy soil, a higher RA/LA was required to limit the negative impact of its high but sensitive $K_{soil\text{-}root}$ on

transpiration. Here, a 50% reduction in maximum transpiration occurred between -0.5 and -1.0 MPa, for a RA/LA of 1 and 7, respectively. At those soil water potentials, rhizosphere and xylem were nearly colimiting $K_{soil\text{-}leaf}$ and thus whole plant water transport. In contrast, in the finest soil analyzed (loam; Fig. 7), $K_{soil\text{-}root}$ did not drive $K_{soil\text{-}leaf}$ and therefore the decline in transpiration became xylem-limited and a function of xylem Ψ_{50}. The soil water potentials at which $K_{soil\text{-}root}$ was reduced by 50% ($\Psi_{soil\text{-}50}$) can also be used as key parameter connecting soil drying to rhizosphere contribution to water uptake, the same way as xylem Ψ_{50} connects plant embolism and $K_{root\text{-}leaf}$ to transpiration (Carminati & Javaux, 2020). It is worth noting that $K_{soil\text{-}root}$ in the model simulations assumes no change in hydraulic conductivity as a function of distance to the root surface (Fig. 7), and therefore underestimates the gradient in water potential around the roots. Eventually, when plants are exposed to severe drying, root shrinkage can create air space between roots and soil and further reduce water movement by decoupling root–soil contact (North & Nobel, 1997; Carminati et al., 2013; Cuneo et al., 2016). However, under severe drought, some species can develop complex rhizosheath (i.e. a layer of adhering soil particle to the root surface bound together by mucilage root exuded either by roots or microorganisms; Price, 1911) to limit air gaps between the roots and the soil and their consequences for the hydraulic conductivity of the root–soil pathway (Delhaize et al., 2015; Basirat et al., 2019). Even though rhizosheaths are present mostly in grasses, crops and desertic plants, some woody plants have been shown to possess an enhanced rhizosheath formation (Pang et al., 2017).

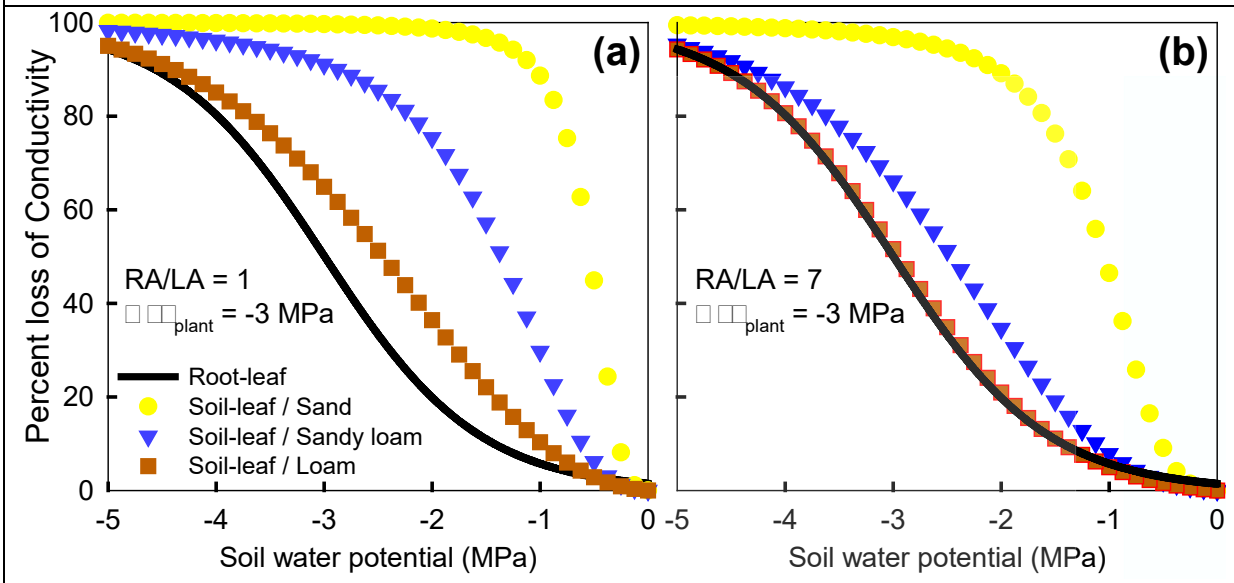

Figure B5. Simulated changes in the percent loss of root to leaf conductance ($K_{root\text{-}leaf}$ that corresponds to whole plant xylem characterized here by a Ψ_{50}, i.e. a mean water potential inducing 50% loss of conductivity, of -3 MPa) and in the percent loss of soil to leaf conductance ($K_{soil\text{-}leaf}$ i.e. vulnerability curves of the whole soil-plant hydraulic pathway) as soil dries in different soils and with root to leaf area ratios (RA/LA) of 1 (a) and 7 (b).

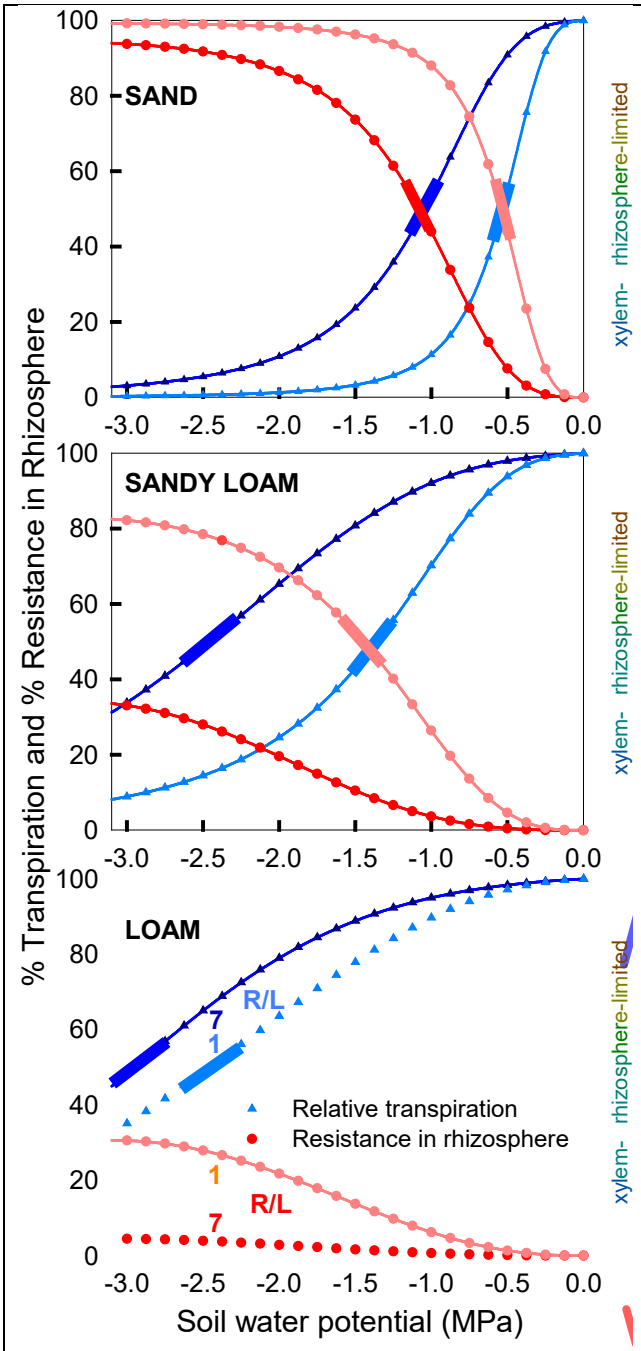

Figure B6. Simulated changes in relative transpiration and in the proportion of the soil to leaf hydraulic resistance ($1/K_{soil\text{-}leaf}$) located in the rhizosphere ($1/K_{soil\text{-}root}$, Figure 5) in different soils and with root area to leaf area ratios (R/L) of 1 (light blue or light red) or 7 (dark blue or dark red). Highlighted blue areas represent the range in soil water potentials inducing 50% (± 5%) loss of transpiration and highlighted red areas those inducing 50% (± 5%) loss of $K_{soil\text{-}root}$ ($\Psi_{soil\text{-}50}$), which can be used to quantify rhizosphere contribution to transpiration as soil dries.

Spatial scales – from organ vulnerability curves to whole plant function

Organ level hydraulic function and dysfunction is now endowed with existing data on thousands of species. Branches, in particular, are well studied with over 2,000 published vulnerability curves (Choat et al., 2012; Hammond et al., in review). However, much fewer studies have been performed on whole-plant and plant-soil hydraulics and vulnerability to hydraulic dysfunction (McCulloh et al., 2019; Cai et al., 2021). This is due to the difficulty of measuring hydraulic failure in intact plants and is particularly difficult in large trees. There are ways to overcome these limitations. During drought experiments, transpiration can be measured having trees in lysimeters and water potentials can be measured with stem psychrometers (Guo et al., 2020; Williams et al., 2021) and soil psychrometers. Control plants can be destructively sampled, and VCs can be obtained from roots, trunks, branches and leaves and soil moisture release curves can be obtained using multiple methods (Jury & Horton, 2004). These types of experiments can resolve where hydraulic failure is occurring during drought and whether it is in the plant or in the soil. The one missing piece of these experiments would be fine roots: if no apparent hydraulic failure was observed in the plant or the soil then fine roots would be the most likely culprit.

In recent years, multiple technologies have been developed for remote sensing of plant water stress. Vegetation water content has been estimated using remote sensing techniques for decades (e.g., Jackson et al., 2004) and new microwave-based methods offer deeper penetration into forest canopies than other methods and are insensitive to cloud cover (Konings et al., 2021). In fact, microwave-based measurements of canopy relative water content were found to be the best predictor of tree mortality in a recent drought in California (Rao et al., 2019). This new development makes remote sensing a tool for monitoring and understanding forest responses to changes in climate in ways never fathomed just a decade earlier. As more new technologies for detecting water content, and potentially, hydraulic function in forests are developed, an understanding of whole-plant-soil hydraulic systems will be even more important for interpreting what remote sensing technologies are revealing about the status of trees.

Conclusion

Catastrophe theory was applied to describe critical or tipping points in simplified dynamical systems representing bubble expansion, embolism spread in xylem network, hydraulic dysfunction, and forest and tree mortality when represented by the von Bertalanffy equation. Similar framework has been successfully employed in the ecological literature but received scant attention in plant hydraulics. The framework described here established links between the critical points and key control variables thereby uncovering generic classes of catastrophes within the xylem system. Control variables such as the size and amount of air molecules in embryonic bubbles that enter a xylem conduit are shown to result in a 'fold' catastrophe. When accounting for cell wall geometry and their mechanical properties to constrain the maximum bubble size transformed the aforementioned fold to a cusp catastrophe. Moving from stability of bubbles within a conduit to spread of bubbles across conduits, it was shown that competition between the ease by which cavitation spreads across xylem conduits and self-limiting controls

693 also lead to a fold catastrophe. The consequences of xylem hydraulics and the control variables
694 describing these catastrophes appear to have minimal impact on the safety-efficiency tradeoff
695 hypothesis. The role of allometric scaling exponents on tipping points within the plant carbon
696 balance was also analyzed and shown to result in a fold catastrophe formed by a transcritical
697 bifurcation when the exponent is different from unity (i.e. the dynamical system must be non-
698 linear). These findings underscore the fact that to move this field and concept forward,
699 connecting structure and processes that are least understood must be undertaken to uncover the
700 nature of nonlinearities in models for the soil-plant continuum. By models of the soil-plant
701 continuum, we mean models that assume continuous water potential from soil to leaf along the
702 chain of interconnected water molecules. These processes include xylem network properties, pit
703 structure and function, belowground hydraulic processes, and whole-plant hydraulics.
704 Strengthening the scientific knowledge around these key aspects of plant hydraulics will enable
705 predictions of tipping points for plant hydraulic failure and mortality when both exogenous and
706 endogenous conditions are gradually altered.

707

708

709

710 **Acknowledgements**

711 The authors thank Kathryn Baker for valuable comments on this paper. This work was supported
712 by NSF-IOS 1754893. The authors have no conflicts of interest.
713

714

715

716

717

718

719

References Cited:

Adams, H.D., Zeppel, M.J., Anderegg, W.R., Hartmann, H., Landhäusser, S.M., Tissue, D.T., Huxman, T.E., Hudson, P.J., Franz, T.E., Allen, C.D. & Anderegg, L.D. (2017) A multi-species synthesis of physiological mechanisms in drought-induced tree mortality. *Nature Ecology and Evolution*, *1*, 1285-1291.

Albuquerque, C., Scoffoni, C., Brodersen, C.R., Buckley, T.N., Sack, L. & McElrone, A.J. (2020) Coordinated decline of leaf hydraulic and stomatal conductances under drought is not linked to leaf xylem embolism for different grapevine cultivars. *Journal of Experimental Botany*, *71*, 7286-7300.

Allen, C.D., Macalady, A.K., Chenchouni, H., Bachelet, D., McDowell, N., Vennetier, M., Kitzberger, T., Rigling, A., Breshears, D.D., Hogg, E.T. & Gonzalez, P. (2010) A global overview of drought and heat-induced tree mortality reveals emerging climate change risks for forests. *Forest Ecology and Management*, *259*, 660-684.

Allen, C.D., Breshears, D.D. & McDowell, N.G. (2015) On underestimation of global vulnerability to tree mortality and forest die-off from hotter drought in the Anthropocene. *Ecosphere*, *6*, 1-55.

Anderegg, W. R. L., Flint, A., Huang, C., Flint, L., Berry, J. A., Davis, F. W., … Field, C.B. (2015) Tree mortality predicted from drought-induced vascular damage. *Nature Geoscience 8*, 367–371.

Anfodillo, T., Carraro, V., Carrer, M., Fior, C., & Rossi, S. (2006) Convergent tapering of xylem conduits in different woody species. *New Phytologist*, *169,* 279-290.

Basirat, M., Mousavi, S.M., Abbaszadeh, S., & Zarebanadkouki, M. (2019) The rhizosheath: a potential root trait helping plants to tolerate drought stress. *Plant Soil 445*, 565–575.

Bertolino, L.T., Caine, R. S., & Gray, J.E. (2019) Impact of Stomatal Density and Morphology on Water-Use Efficiency in a Changing World. *Frontiers in Plant Science 10*, 225

Briggs, LJ. (1950) Limiting negative pressure of water. *Journal of Applied Physics. 21,* 721–722.

Brodersen, C.R., Choat, B., Chatelet, D.S., Shackel, K.A., Matthews, M.A., & McElrone, A.J. (2013) Xylem vessel relays contribute to radial connectivity in grapevine stems (Vitis vinifera and V. arizonica; Vitaceae). *American Journal of Botany*, *100*, 314-321.

Brodersen, C.R., Knipfer, T., & McElrone, A.J. (2018) In vivo visualization of the final stages of xylem vessel refilling in grapevine (Vitis vinifera) stems. *New Phytologist*, *217*, 117-126.

Brodribb, T. J., Powers, J., Cochard, H., & Choat, B. (2020). Hanging by a thread? Forests and drought. *Science 368*, 261–266.

Brooks, R.H., & Corey, A.T. (1964) Hydraulic properties of porous media and their relation to drainage design. *Transactions of the ASAE*, *7*, 26-28.

Cai, G., Carminati, A., Abdalla, M., & Ahmed, M.A. (2021) Soil textures rather than root hairs dominate water uptake and soil–plant hydraulics under drought. *Plant Physiology*, *187*, 858-872.

Campbell, G.S. (1985) Soil Physics with Basic; Transport Models or Soil-Plant Systems. Elsevier Science Publishers, Amsterdam.

Capron, M., Tordjeman, P., Charru, F., Badel, E., & Cochard, H. (2014) Gas flow in plant microfluidic networks controlled by capillary valves. *Physical Review E 89*, 033019.

763 Carlquist, S. (1985) Vasicentric tracheids as a drought survival mechanism in the woody flora of
764 southern California and similar regions; review of vasicentric tracheids. *Aliso: A Journal*
765 *of Systematic and Evolutionary Botany*, *11*, 37-68.
766 Carminati, A., Vetterlein, D., Koebernick, N., Blaser, S., Weller, U., & Vogel, H. J. (2013) Do
767 roots mind the gap? *Plant Soil 367*, 651–661.
768 Carminati A., & Javaux, M. (2020) Soil Rather Than Xylem Vulnerability Controls Stomatal
769 Response to Drought. *Trends in Plant Science 25*, 868-880.
770 Chaumont, F., & Tyerman, S. D. (2014) Aquaporins: highly regulated channels controlling plant
771 water relations. *Plant Physiology 164*, 1600–1618.
772 Choat, B., Jansen, S., Brodribb, T.J., Cochard, H., Delzon, S., Bhaskar, R., Bucci, S.J., Feild,
773 T.S., Gleason, S.M., Hacke, U.G., & Jacobsen, A.L. (2012) Global convergence in the
774 vulnerability of forests to drought. *Nature*, *491*, 752-755.
775 Christman, M.A., Sperry, J.S., & Adler, F.R. (2009) Testing the 'rare pit' hypothesis for xylem
776 cavitation resistance in three species of Acer. *New Phytologist 182*, 664-674.
777 Comstock, G.L., & Côté, W.A., (1968) Factors affecting permeability and pit aspiration in
778 coniferous sapwood. *Wood Science and Technology*, *2*, 279-291.
779 Cuneo, I., Knipfer, T., Brodersen, C., & McElrone, A. (2016) Mechanical failure of fine root
780 cortical cells initiates plant hydraulic declined during drought. *Plant Physiology*, *172*,
781 1669–1678.
782 Darwin, F., Vines, S.H., Joly, J., & FitzGerald, G.F. (1896) Report of a discussion on the ascent
783 of water in trees. *Annals of Botany 10*, 630-661
784 Delhaize, E., Rathjen, T.M., & Cavanagh, C.R. (2015) The genetics of rhizosheath size in a
785 multiparent mapping population of wheat. *Journal of Experimental Botany 66*, 4527–
786 4536.
787 Delzon, S., Douthe, C., Sala, A, & Cochard, H. (2010**)** Mechanism of water-stress induced
788 cavitation in conifers: bordered pit structure and function support the hypothesis of seal
789 capillary-seeding. *Plant Cell Environment 33,* 2101-2111.
790 Dietze, M.C., & Moorcroft, P.R. (2011) Tree mortality in the eastern and central United States:
791 patterns and drivers. *Global Change Biology*, *17*, 3312-3326.
792 Dittmer, H. J. (1949) Root Hair Variations in Plant Species. *American Journal of Botany*, *36*, 152–
793 155.
794 Domec, J.C., & Gartner, B.L. (2001) Cavitation and water storage capacity in bole xylem
795 segments of mature and young Douglas-fir trees. *Trees*, *15*, 204-214.
796 Domec, J.C., Lachenbruch, B.L., & Meinzer, F.C. (2006) Bordered pit structure and function
797 determine spatial patterns of air-seeding thresholds in xylem of Douglas-fir (*Pseudostuga*
798 *menziesii*; Pinaceae) trees. *American Journal of Botany* 93, 1588-1600.
799 Domec, J.C., Noormets, A., King, J.S., Sun, G., McNulty, S.G., Gavazzi, M.J., Boggs, J., &
800 Treasure, E.A. (2009) Decoupling the influence of leaf and root hydraulic conductances on
801 stomatal conductance and its sensitivity to vapour pressure deficit as soil dries in a drained
802 loblolly pine plantation. *Plant Cell Environment 32*, 980–991.
803 Domec, J.C., King, J.S., Carmichael, M.J., Overby, A.T., Wortemann, R.R., K Smith, W., Miao,
804 G., Noormets, A., & Johnson, D.M. (2021) Root water gates and not changes in root
805 structure provide new insights into plant physiological responses to drought, flooding and
806 salinity. *Journal of Experimental Botany 72*, 4489-4501.

807 Doussan, C., Vercambr, G., & Page, L. (1998) Modelling of the Hydraulic Architecture of Root
808 Systems: An Integrated Approach to Water Absorption—Distribution of Axial and Radial
809 Conductances in Maize. *Annals of Botany 81*, 225–232.
810 Draye, X., Kim, Y., Lobet, G., & Javaux, M. (2010) Model-assisted integration of physiological
811 and environmental constraints affecting the dynamic and spatial patterns of root water
812 uptake from soils. *Journal of Experimental Botany 61*, 2145–2155.
813 Duan, C., Karnik, R., Lu, M.C., & Majumdar, A. (2012) Evaporation-induced cavitation in
814 nanofluidic channels. *Proceedings of the National Academy of Sciences*, *109*, 3688-3693.
815 Dublin, H.T., Sinclair, A.R., & McGlade, J. (1990) Elephants and fire as causes of multiple
816 stable states in the Serengeti-Mara woodlands. *The Journal of Animal Ecology*, *59*, 1147-
817 1164.
818 Ehlert, C., Maurel, C., Tardieu, F., & Simonneau, T. (2009) Aquaporin-mediated reduction in
819 maize root hydraulic conductivity impacts cell turgor and leaf elongation even without
820 changing transpiration. *Plant Physiology 150*, 1093–1104.
821 Ewers, B.E., Oren, R., & Sperry, J.S. (2000) Influence of nutrient versus water supply on
822 hydraulic architecture and water balance in Pinus taeda. *Plant Cell Environment*, *23*,
823 1055-1066.
824 Feng, F., Losso, A., Tyree, M., Zhang, S., & Mayr, S. (2021) Cavitation fatigue in conifers: a
825 study on eight European species. *Plant Physiology 186*, 1580-1590.
826 Givnish, T.J., & Vermeij, G.J. (1976) Sizes and shapes of liane leaves. *The American Naturalist*,
827 *110*, 743-778.
828 Guo, J.S., Hultine, K.R., Koch, G.W., Kropp, H., & Ogle, K. (2020) Temporal shifts in
829 iso/anisohydry revealed from daily observations of plant water potential in a dominant
830 desert shrub. *New Phytologist*, *225*, 713-726.
831 Guswa, A.J. (2008) The influence of climate on root depth: A carbon cost-benefit analysis.
832 *Water Resources Research*, *44*, W02427.
833 Hacke, U.G., Sperry, J.S., Ewers, B.E., Ellsworth, D.S., Schäfer, K.V.R., & Oren, R. (2000)
834 Influence of soil porosity on water use in Pinus taeda. *Oecologia*, *124*, 495-505.
835 Hacke, U.G., Stiller, V., Sperry, J.S., Pittermann, J., & McCulloh, K.A. (2001) Cavitation
836 fatigue. Embolism and refilling cycles can weaken the cavitation resistance of xylem.
837 *Plant Physiology*, *125*, 779-786.
838 Hacke, U.G., Sperry, J.S., & Pittermann, J. (2004) Analysis of circular bordered pit function II.
839 Gymnosperm tracheids with torus-margo pit membranes. *American Journal of Botany*,
840 *91*, 386-400.
841 Hammond, W.M., Yu, K., Wilson, L.A., Will, R.E., Anderegg, W.R., & Adams, H.D. (2019)
842 Dead or dying? Quantifying the point of no return from hydraulic failure in drought-
843 induced tree mortality. *New Phytologist*, *223*, 1834-1843.
844 Hammond, W.M., Johnson, D.M., & Meinzer, F.C. (2021) A thin line between life and death:
845 radial sap flux failure signals trajectory to tree mortality. *Plant Cell Environment*, *44*,
846 1311-1314.
847 Hillabrand, R.M., Hacke, U.G., & Lieffers, V.J. (2016) Drought-induced xylem pit membrane
848 damage in aspen and balsam poplar. *Plant Cell Environment*, *39*, 2210-2220.
849 Holbrook, N.M., & Zwieniecki, M.A. (1999) Embolism repair and xylem tension. Do we need a
850 miracle? *Plant Physiology, 120*, 7–10.
851 Hölttä, T., Vesala, T., & Nikinmaa, E. (2007) A model of bubble growth leading to xylem
852 conduit embolism. *Journal of Theoretical Biology*, *249*, 111-123.

Hsiao, T.C. (1973) Plant Responses to Water Stress. *Annual Review of Plant Physiology, 24*, 519-570

Huang, C.W., Domec, J.C., Ward, E.J., Duman, T., Manoli, G., Parolari, A.J., & Katul, G.G., (2017) The effect of plant water storage on water fluxes within the coupled soil–plant system. *New Phytologist*, *213*, 1093-1106.

Hunt, A. G. (2005) Basic transport properties in natural porous media. *Complexity*, 10(1), 22-37

Jackson, T.J., Chen, D., Cosh, M., Li, F., Anderson, M., Walthall, C., Doriaswamy, P., & Hunt, E.R. (2004) Vegetation water content mapping using Landsat data derived normalized difference water index for corn and soybeans. *Remote Sensing of Environment*, *92*, 475-482.

Jansen, S., Lamy, J.B., Burlett, R., Cochard, H., Gasson, P., & Delzon, S. (2012) Plasmodesmatal pores in the torus of bordered pit membranes affect cavitation resistance of conifer xylem. *Plant Cell Environment*, *35*, 1109-1120.

Jensen, K.H., Berg-Sørensen, K., Bruus, H., Holbrook, N.M., Liesche, J., Schulz, A., Zwieniecki, M.A., & Bohr, T. (2016) Sap flow and sugar transport in plants. *Reviews of Modern Physics*, *88*, 035007.

Johnson, D.M., Brodersen, C.R., Reed, M., Domec, J.C., & Jackson, R.B. (2014) Contrasting hydraulic architecture and function in deep and shallow roots of two co-occurring tree species from an arid habitat. *Annals of Botany 113*, 617-627.

Johnson, D.M., Wortemann, R., McCulloh, K.A., Jordan-Meille, L., Ward, E., Warren, J.M., Palmroth, S., & Domec, J.C. (2016) A test of the hydraulic vulnerability segmentation hypothesis in angiosperm and conifer tree species. *Tree physiology*, *36*, 983-993.

Johnson, D.M., Domec, J.C., Berry, Z.C., Schwantes, A.M., McCulloh, K.A., Woodruff, D.R., Polley, W.H., Wortemann, R., Swenson, J.J., Mackay, D.S., & McDowell, N.G. (2018) Co-occurring woody species have diverse hydraulic strategies and mortality rates during an extreme drought. *Plant Cell Environment*, *41*, 576-588.

Jury, W.A., & Horton, R. (2004) *Soil Physics*. John Wiley & Sons.

Kaack, L. H., & Katul, G. G. (2013). Fifty years to prove Malthus right. *Proceedings of the National Academy of Sciences*, *110*(11), 4161-4162

Kaack, L., Weber, M., Isasa, E., Karimi, Z., Li, S., Pereira, L., Trabi, C.L., Zhang, Y., Schenk, H.J., Schuldt, B., & Schmidt, V. (2021) Pore constrictions in intervessel pit membranes provide a mechanistic explanation for xylem embolism resistance in angiosperms. *New Phytologist* (online early)

Katul, G., Manzoni, S., Palmroth, S., & Oren, R. (2010) A stomatal optimization theory to describe the effects of atmospheric CO2 on leaf photosynthesis and transpiration. *Annals of Botany*, *105*, 431-442.

Katul, G.G., Mrad, A., Bonetti, S., Manoli, G., & Parolari, A. J. (2020) Global convergence of COVID-19 basic reproduction number and estimation from early-time SIR dynamics. *PLoS One*, 15(9), e0239800

Konings, A. G., Katul, G. G., & Porporato, A. (2010). The rainfall-no rainfall transition in a coupled land-convective atmosphere system. *Geophysical Research Letters*, *37*, L14401.

Konings, A.G., Saatchi, S.S., Frankenberg, C., Keller, M., Leshyk, V., Anderegg, W.R., Humphrey, V., Matheny, A.M., Trugman, A., Sack, L., & Agee, E., 2021. Detecting Forest Response to Droughts with Global Observations of Vegetation Water Content. *Global Change Biology*, *27*, 6005-6024.

Konrad, W., & Roth-Nebelsick, A. (2003) The dynamics of gas bubbles in conduits of vascular plants and implications for embolism repair. *Journal of Theoretical Biology*, *224*, 43-61.
Konrad, W., & Roth-Nebelsick, A. (2005). The significance of pit shape for hydraulic isolation of embolized conduits of vascular plants during novel refilling. *Journal of Biological Physics*, *31*, 57-71.
Konrad, W., & Roth-Nebelsick, A. (2006) Embolism formation and repair in vascular plants: the role of cell wall mechanics. In *Proceedings of the 5th Plant Biomechanics Conference, Editor: Lennart Salmn, Stockholm* (p. 417422).
Konrad, W., & Roth-Nebelsick, A (2009) November. The influence of the wall contact angle on gas bubble behaviour in xylem conduits under tension and possible consequences for embolism. In *Proceedings of the Sixth Plant Biomechanics Conference. Institut für Angewandte Physik, Vienna* (pp. 32-39).
Konrad, W., Katul, G., Roth-Nebelsick, A., & Jensen, K. H. (2019). Xylem functioning, dysfunction and repair: a physical perspective and implications for phloem transport. *Tree Physiology*, *39*, 243-261.
Körner, C. (2019) No need for pipes when the well is dry—a comment on hydraulic failure in trees. *Tree Physiology*, *39*, 695-700.
Kotowska, M.M., Thom, R., Zhang, Y., Schenk, H.J., & Jansen, S. (2020) Within-tree variability and sample storage effects of bordered pit membranes in xylem of Acer pseudoplatanus. *Trees*, *34*, 61-71.
Knowlton, N. (1992) Thresholds and multiple stable states in coral reef community dynamics. *American Zoologist*, *32*, 674-682.
Lamacque, L., Charrier, G., Farnese, F. D. S., Lemaire, B., Améglio, T., & Herbette, S. (2020). Drought-induced mortality: Branch diameter variation reveals a point of no recovery in lavender species. *Plant Physiology, 183*, 1638–1649.
Lersten, N.R. (1997) Occurrence of endodermis with a casparian strip in stem and leaf. *The Botanical Review*, *63*, 265-272.
Liesche, J., Vincent, C., Han, X., Zwieniecki, M., Schulz, A., Gao, C., Bravard, R., Marker, S., & Bohr, T. (2021) The mechanism of sugar export from long conifer needles. *New Phytologist*, *230*, 1911-1924.
Liu, Y., Kumar, M., Katul, G. G., & Porporato, A. (2019). Reduced resilience as an early warning signal of forest mortality. *Nature Climate Change*, *9*, 880-885.
Liu, Y., Kumar, M., Katul, G. G., Feng, X., & Konings, A. G. (2020). Plant hydraulics accentuates the effect of atmospheric moisture stress on transpiration. *Nature Climate Change*, *10*, 691-695.
Loepfe, L., Martinez-Vilalta, J., Piñol, J., & Mencuccini, M. (2007) The relevance of xylem network structure for plant hydraulic efficiency and safety. *Journal of Theoretical Biology*, *247*, 788-803.
Ludwig, D., Jones, D. D., & Holling, C. S. (1978) Qualitative analysis of insect outbreak systems: the spruce budworm and forest. *The Journal of Animal Ecology*, *47*, 315-332.
Manoli, G., Bonetti, S., Domec, J. C., Putti, M., Katul, G., & Marani, M. (2014) Tree root systems competing for soil moisture in a 3D soil–plant model. *Advances in Water Resources*, *66*, 32-42.
Manoli, G., Huang, C. W., Bonetti, S., Domec, J. C., Marani, M., & Katul, G. (2017). Competition for light and water in a coupled soil-plant system. *Advances in Water Resources*, *108*, 216-230.

Manzoni, S., Vico, G., Katul, G., Palmroth, S., Jackson, R.B., & Porporato, A. (2013) Hydraulic limits on maximum plant transpiration and the emergence of the safety–efficiency trade-off. *New Phytologist*, *198*, 169-178.

Manzoni, S., Katul, G., & Porporato, A. (2014) A dynamical system perspective on plant hydraulic failure. *Water Resources Research*, *50*, 5170-5183.

Maurel, C., & Prado, K. (2017) Aquaporins and leaf water relations. In *Plant aquaporins*, pp. 155-165. Springer.

McCulloh, K., Sperry, J.S., Lachenbruch, B., Meinzer, F.C., Reich, P.B., & Voelker, S. (2010) Moving water well: comparing hydraulic efficiency in twigs and trunks of coniferous, ring-porous, and diffuse-porous saplings from temperate and tropical forests. *New Phytologist*, *186*, 439-450.

McCulloh, K.A., Domec, J.C., Johnson, D.M., Smith, D.D., & Meinzer, F.C. (2019) A dynamic yet vulnerable pipeline: Integration and coordination of hydraulic traits across whole plants. *Plant Cell Environment*, *42*, 2789-2807.

McCully M.E. (1999). Roots in Soil: Unearthing the complexities of roots and their rhizospheres. *Annual Review of Plant Physiology and Plant Molecular Biology 50,* 695-718.

Meinzer, F.C., Johnson, D.M., Lachenbruch, B., McCulloh, K.A., & Woodruff, D.R. (2009) Xylem hydraulic safety margins in woody plants: coordination of stomatal control of xylem tension with hydraulic capacitance. *Functional Ecology*, *23*, 922-930.

Meyra, A. G., Zarragoicoechea, G. J., & Kuz, V. A. (2011). A similarity law in botanic. The case of hydraulic conductivity of trees. *The European Physical Journal D*, *62*, 19-23.

Millburn J.A., & Johnson R.P.C. (1966) The conduction of sap. I. Detection of vibrations produced by sap cavitation in *Ricinus* xylem. *Planta 69,* 43–52.

Moshelion, M., Halperin, O., Wallach, R., Oren, R., & Way, D.A. (2015) Role of aquaporins in determining transpiration and photosynthesis in water-stressed plants: crop water-use efficiency, growth and yield. *Plant Cell Environment*, *38*, 1785-1793.

Mrad, A., Domec, J. C., Huang, C. W., Lens, F., & Katul, G. (2018). A network model links wood anatomy to xylem tissue hydraulic behaviour and vulnerability to cavitation. *Plant Cell Environment*, *41*, 2718-2730.

Mrad, A., Sevanto, S., Domec, J. C., Liu, Y., Nakad, M., & Katul, G. (2019). A dynamic optimality principle for water use strategies explains isohydric to anisohydric plant responses to drought. *Frontiers in Forests and Global Change*, *2*, 49.

Mrad, A., Manzoni, S., Oren, R., Vico, G., Lindh, M., & Katul, G. (2020). Recovering the metabolic, self-thinning, and constant final yield rules in mono-specific stands. *Frontiers in Forests and Global Change*, *3*, 62.

Mrad A., Johnson, D.M., Love, D.M., & Domec, J.C. (2021) The roles of conduit redundancy and connectivity in xylem hydraulic functions. *New Phytologist, 231*, 996-1007.

Nobel, P.S., & Cui, M. (1992). Hydraulic conductances of the soil, the root-sol air gap, and the root: changes for desert succulents in drying soil. *Journal of Experimental Botany, 43*, 319-326.

North, G.B., & Nobel, P.S. (1997) Drought-induced changes in soil contact and hydraulic conductivity for roots of Opuntia ficus-indica with and without rhizosheaths. *Plant and Soil, 191,* 249–258.

Oertli, J. J. (1971) The stability of water under tension in the xylem. *Zeitschrift PJlanzen physiologie, 65*, 195-209.

Ogle, K., Barber, J.J., Willson, C., & Thompson, B. (2009) Hierarchical statistical modeling of xylem vulnerability to cavitation. *New Phytologist, 182*, 541–554

Olson, M.E., Anfodillo, T., Gleason, S.M., & McCulloh, K.A. (2021) Tip-to-base xylem conduit widening as an adaptation: causes, consequences, and empirical priorities. *New Phytologist*, *229*, 1877-1893.

Pammenter, N.W., & Vander Willigen, C. (1998) A mathematical and statistical analysis of the curves illustrating vulnerability of xylem to cavitation. *Tree Physiology, 18*, 589–593

Pang, J., Ryan, M.H., Siddique, K.H., & Simpson, R.J. (2017). Unwrapping the rhizosheath. *Plant and Soil, 418*, 129-139.

Parolari, A. J., Katul, G. G., & Porporato, A. (2014). An ecohydrological perspective on drought-induced forest mortality. *Journal of Geophysical Research: Biogeosciences*, *119*, 965-981.

Parolari, A. J., Katul, G. G., & Porporato, A. (2015). The Doomsday Equation and 50 years beyond: new perspectives on the human-water system. *Wiley Interdisciplinary Reviews: Water*, *2*, 407-414.

Passioura, J.B. (1988) Water Transport in and to Roots. *Annual Reviews in Plant Physiology, 39*, 245-265

Percolla, M.I., Fickle, J.C., Rodríguez-Zaccaro, F.D., Pratt, R.B., & Jacobsen, A.L. (2021) Hydraulic function and conduit structure in the xylem of five oak species. *IAWA Journal*, *43,* 279-298.

Perry, D. A. (1984) A model of physiological and allometric factors in the self-thinning curve. *Journal of Theoretical Biology*, *106*, 383-401.

Pfautsch, S., Renard, J., Tjoelker, M.G., & Salih, A. (2015) Phloem as capacitor: radial transfer of water into xylem of tree stems occurs via symplastic transport in ray parenchyma. *Plant Physiology*, *167*, 963-971.

Pittermann, J., Sperry, J.S., Hacke, U.G., Wheeler, J.K., & Sikkema, E.H. (2006) Inter-tracheid pitting and the hydraulic efficiency of conifer wood: the role of tracheid allometry and cavitation protection. *American Journal of Botany*, *93*, 1265-1273.

Plesset, M. S., & Prosperetti, A. (1977) Bubble dynamics and cavitation. *Annual Review of Fluid Mechanics*, 9(1), 145-185.

Preisler, Y., Tatarinov, F., Grünzweig, J. M., & Yakir, D. (2021) Seeking the "point of no return" in the sequence of events leading to mortality of mature trees. *Plant Cell Environment, 44*, 1315–1328.

Price, S.R. (1911) The Roots of Some North African Desert-Grasses. *New Phytologist, 10*, 328–40.

Rao, K., Anderegg, W.R., Sala, A., Martínez-Vilalta, J., & Konings, A.G. (2019) Satellite-based vegetation optical depth as an indicator of drought-driven tree mortality. *Remote Sensing of Environment*, *227*,125-136.

Roth-Nebelsick, A. (2019) It's contagious: calculation and analysis of xylem vulnerability to embolism by a mechanistic approach based on epidemic modeling. *Trees, 33*, 1519–1533

Rowland, L., da Costa, A.C.L., Galbraith, D.R., Oliveira, R.S., Binks, O.J., Oliveira, A.A.R., Pullen, A.M., Doughty, C.E., Metcalfe, D.B., Vasconcelos, S.S., & Ferreira, L.V. (2015) Death from drought in tropical forests is triggered by hydraulics not carbon starvation. *Nature*, *528*, 119-122.

Scheffer, M., Carpenter, S., Foley, J.A., Folke, C.m & Walker, B. (2001) Catastrophic shifts in ecosystems. *Nature*, *413*, 591-596.

Scheffer, M., & Carpenter, S.R. (2003) Catastrophic regime shifts in ecosystems: linking theory to observation. *Trends in Ecology & Evolution, 18*, 648-56.

Schenk, H.J., Espino, S., Goedhart, C.M., Nordenstahl, M., Cabrera, H.I.M., & Jones, C.S. (2008) Hydraulic integration and shrub growth form linked across continental aridity gradients. *Proceedings of the National Academy of Sciences*, *105*, 11248-11253.

Schulte, P. J., & Hacke, U. G. (2021). Solid mechanics of the torus–margo in conifer intertracheid bordered pits. *New Phytologist*, *229*, 1431-1439.

Sevanto, S., Hölttä, T., & Holbrook, N.M. (2011) Effects of the hydraulic coupling between xylem and phloem on diurnal phloem diameter variation. *Plant Cell Environment*, *34*, 690-703.

Sevanto, S., Mcdowell, N.G., Dickman, L.T., Pangle, R., & Pockman, W.T. (2014) How do trees die? A test of the hydraulic failure and carbon starvation hypotheses. *Plant Cell Environment*, *37*, 153-161.

Shatil-Cohen, A., Attia, Z., & Moshelion, M. (2011) Bundle-sheath cell regulation of xylem-mesophyll water transport via aquaporins under drought stress: a target of xylem-borne ABA?. *The Plant Journal*, *67*, 72-80.

Shen, F., Gao, R., Liu, W., & Zhang, W. (2002) Physical analysis of the process of cavitation in xylem sap. *Tree Physiology*, *22*, 655-659.

Shen, F., Wenji, L., Rongfu, G., & Hu, H. (2003) A careful physical analysis of gas bubble dynamics in xylem. *Journal of Theoretical Biology*, *225*, 229-233.

Shen, F., Wang, Y., Cheng, Y., & Zhang, L. (2012) Three types of cavitation caused by air seeding. *Tree Physiology*, *32*, 1413-141

Siqueira, M., Katul, G., & Porporato, A. (2008) Onset of water stress, hysteresis in plant conductance, and hydraulic lift: Scaling soil water dynamics from millimeters to meters. *Water Resources Research*, *44*, W01432.

Sornette, D. (2002) Predictability of catastrophic events: Material rupture, earthquakes, turbulence, financial crashes, and human birth. *Proceedings of the National Academy of Sciences*, *99*, 2522-2529.

Strogatz, S.H. (1994) Nonlinear dynamics and chaos: with applications to physics. *Biology, Chemistry and Engineering*, 498 pp. Addison-Wesley Publishing, Boston

Sperry, J.S., & Tyree, M.T. (1988) Mechanism of water-stress-induced xylem embolism. *Plant Physiology, 88*, 581–587

Sperry, J.S., Nichols, K.L., Sullivan, J.E., & Eastlack, S.E. (1994) Xylem embolism in ring-porous, diffuse-porous, and coniferous trees of northern Utah and interior Alaska. *Ecology*, *75*, 1736-1752.

Sperry, J.S., Adler, F.R., Campbell, G.S., & Comstock, J.P. (1998) Limitation of plant water use by rhizosphere and xylem conductance: Results from a model. *Plant Cell Environment 21,* 347–359.

Sperry, J.S. (2000) Hydraulic constraints on plant gas exchange. *Agricultural and Forest Meteorology*, *104*, 13-23.

Sperry, J.S., & U.G. Hacke (2004) Analysis of circular bordered pit function. I. Angiosperm vessels with homogenous pit membranes. *American Journal of Botany, 91*, 369–385

Sperry, J.S., Hacke, U.G., & Wheeler, J.K. (2005) Comparative analysis of end wall resistivity in xylem conduits. *Plant Cell Environment*, *28*, 456-465.

Sperry, J.S., Hacke, U.G., & Pittermann, J. (2006) Size and function in conifer tracheids and angiosperm vessels. *American Journal of Botany*, *93*, 1490-1500.

Sperry, J.S., & Love, D.M. (2015) What plant hydraulics can tell us about plant responses to climate-change droughts. *New Phytologist, 207*, 14-27

Sperry, J.S., Venturas, M.D., Anderegg, W.R., Mencuccini, M., Mackay, D.S., Wang, Y., & Love, D.M. (2017) Predicting stomatal responses to the environment from the optimization of photosynthetic gain and hydraulic cost. *Plant Cell Environment*, *40*, 816-830.

Steudle, E. (1994) Water transport across roots. *Plant and Soil*, *167*, 79-90.

Teskey, R.O., Hinckley, T.M., & Grier, C.C. (1983) Effect of interruption of flow path on stomatal conductance of Abies amabilis. *Journal of Experimental Botany*, *34*, 1251-1259.

Thom, R. (1975) Structural stability and morphogenesis (translated by DH Fowler).

Tibbetts, T.J., & Ewers, F.W. (2000) Root pressure and specific conductivity in temperate lianas: exotic Celastrus orbiculatus (Celastraceae) vs. native Vitis riparia (Vitaceae). *American Journal of Botany*, *87*, 1272-1278.

Tixier, A., Herbette, S., Jansen, S., Capron, M., Tordjeman, P., Cochard, H., & Badel, E. (2014) Modelling the mechanical behaviour of pit membranes in bordered pits with respect to cavitation resistance in angiosperms. *Annals of Botany*, *114*, 325-334.

Trueba, S., Théroux-Rancourt, G., Earles, J.M., Buckley, T.N., Love, D.M., Johnson, D.M., & Brodersen, C. (2021) The 3d construction of leaves is coordinated with water use efficiency in conifers. *New Phytologist* (in press)

Trugman, A. T., Anderegg, L. D. L., Anderegg, W. R. L., Das, A. J., & Stephenson, N. L. (2021). Why is tree drought mortality so hard to predict? *Trends in Ecology and Evolution, 36*, 520–532.

Tsuda, M., & Tyree, M.T. (1997) Whole-plant hydraulic resistance and vulnerability segmentation in Acer saccharinum. *Tree Physiology, 17,* 351-357.

Tyree, M.T., Cochard, H., Cruiziat, P., Sinclair, B., & Ameglio, T. (1993) Drought-induced leaf shedding in walnut: evidence for vulnerability segmentation. *Plant Cell Environment 16*, 879-882

Tyree, M.T., & Sperry, J.S. (1989) Vulnerability of xylem to cavitation and embolism. *Annual Review of Plant Biology*, *40*, 19-36.

Umebayashi, T., Morita, T., Utsumi, Y., Kusumoto, D., Yasuda, Y., Haishi, T., & Fukuda, K., (2016) Spatial distribution of xylem embolisms in the stems of Pinus thunbergii at the threshold of fatal drought stress. *Tree Physiology*, *36*, 1210-1218.

Umebayashi, T., Sperry, J.S., Smith, D.D., & Love, D.M. (2019) 'Pressure fatigue': the influence of sap pressure cycles on cavitation vulnerability in Acer negundo. *Tree Physiology*, *39*, 740-746.

Van den Honert, T. (1948) Water transport in plants as a catenary process. *Discussions of the Faraday Soc*iety, *3*, 146-153

van Genuchten, M.T. (1980) A closed-form equation for predicting the hydraulic conductivity of unsaturated soils. *Soil Science Society of America Journal, 44*, 892-898

Von Bertalanffy, L. (1938) A quantitative theory of organic growth (inquiries on growth laws. II). *Human Biology*, *10*, 181-213.

Von Foerster, H., Mora, P.M., & Amiot, L.W. Doomsday: Friday, 13 November, AD 2026. *Science, 132*, 1291-1295.

Wheeler, J. K., Sperry, J. S., Hacke, U. G., & Hoang, N. (2005). Inter-vessel pitting and cavitation in woody Rosaceae and other vesselled plants: a basis for a safety versus efficiency trade-off in xylem transport. *Plant Cell Environment*, *28*, 800-812.

Williams, C.B., Næsborg, R.R., Ambrose, A.R., Baxter, W.L., Koch, G.W., & Dawson, T.E., (2021) The dynamics of stem water storage in the tops of Earth's largest trees—Sequoiadendron giganteum. *Tree Physiology* (in press).
Zanne, A.E., Sweeney, K., Sharma, M., & Orians, C.M. (2006) Patterns and consequences of differential vascular sectoriality in 18 temperate tree and shrub species. *Functional Ecology*, *20*, 200-206.
Zeeman, E.C. (1976) Catastrophe theory. *Scientific American*, *234*, 65-83.
Zeeman, E.C. (1978) Catastrophe and Psychology. Royal Institution of Great Britain. https://www.rigb.org/christmas-lectures/watch/1978/mathematics-into-pictures/catastrophe-and-psychology
Zelinka, S.L., Bourne, K.J., Hermanson, J.C., Glass, S.V., Costa, A., & Wiedenhoeft, A.C. (2015) Force–displacement measurements of earlywood bordered pits using a mesomechanical tester. *Plant Cell Environment*, *38*, 2088-2097.
Zhang, Y., Klepsch, M., & Jansen, S. (2017) Bordered pits in xylem of vesselless angiosperms and their possible misinterpretation as perforation plates. *Plant Cell Environment*, *40*, 2133-2146.
Zhang, Y., Carmesin, C., Kaack, L., Klepsch, M.M., Kotowska, M., Matei, T., Schenk, H.J., Weber, M., Walther, P., Schmidt, V., & Jansen, S. (2020) High porosity with tiny pore constrictions and unbending pathways characterize the 3D structure of intervessel pit membranes in angiosperm xylem. *Plant Cell Environment*, *43*, 116-130.
Zimmerman, M.H., & Brown, C.L. (1971) *Trees: structure and function*. New York, USA, Springer-Verlag.
Zimmermann, M.H. (1983) Xylem structure and the ascent of sap. Springer-Verlag, Berlin.
Zwieniecki, M.A., & Holbrook, N.M. (2000) Bordered pit structure and vessel wall surface properties. Implications for embolism repair. *Plant Physiology, 123*, 1015–1020

1153 Table 1: Symbols and definitions
1154

A	area
A_c	the proportion of photosynthates allocated to above ground tissue
α	is equal to: $A_c\ P_g\ c/k_m$
B	above-ground biomass
B_{eq}	above-ground biomass at equilibrium
b and b'	how easily an impaired vessel embolizes a water-filled one
c	the median pressure necessary for air entry into the biggest pores of the population of pit-fields or leaf area scaling parameter in VBE
c_a	atmospheric CO_2 concentration
c_i	intercellular CO_2 concentration
d	related to the coefficient of variation of the maximum pore population of pit-fields
d_t	cell wall thickness
E_t	Young's modulus of elasticity
γ	surface tension coefficient of liquid water
h	path length from root to leaf
k_m	is rate of maintenance respiration plus tissue death
K_{max}	maximum hydraulic conductivity of the xylem
K_{sat}	Saturated soil conductivity
k_n	probability of finding an embolized vessel
K_{soil}, K_{root}, *etc.*	hydraulic conductivity of soil, root, etc.
L	leaf area
l_t	tracheid length
LAI	leaf area index
μ	cell-wall material compressibility
n	number of molecules; also scaling exponent in VBE
n_{max}	maximum number of molecules
p	pressure
p^*	saturation vapor pressure
p_s	xylem pressure
ψ	xylem tension
ψ_l	leaf tension
ψ_o	reference xylem tension
ψ_{soil}	soil water potential
ψ_{xylem}	xylem water potential
ψ_{12}	xylem tension (water potential) at 12% loss of conductivity
ψ_{50}	xylem tension (water potential) at 50% loss of conductivity
P_g	gross photosynthesis per unit leaf area reduced by photorespiration and synthesis respiration
PLC	per cent loss of conductivity
R	radius
RAI	root area index
RLD	root length density

R_e	threshold radius for bubble expansion
R_m	maximum bubble radius
r_{root}	root radius
r_{soil}	soil radial distance from the roots to the mean distance between roots
r_t	undeformed tracheid radius
$\Re$	universal gas constant
σ_t	Poisson number
t	time
T	temperature
T_r	transpiration
θ	contact angle
V	volume
$V(B)$	potential surface in VBE
VC	vulnerability curve
VPD	vapor pressure deficit
W	principal Lambert W-function
WUE	leaf-scale water use efficiency

1155